Rijksuniversiteit Groningen

Bachelor Thesis

Potential Constraints from a $B_c \to \tau\nu_\tau$ Measurement on the New Physics Parameter Space

Author:
BSc. A.F. Esselink

Supervisor:
dr. K.A.M. de Bruyn

Date:
07/07/2023

Abstract

B meson decays containing leptons can offer important insights into physics beyond the Standard Model through comparison of experimental measurements and their SM estimates. Using the method presented in Fleischer *et al.*, 2021, observables containing ratios of B meson decays and their experimental measurements were used to constrain the Wilson coefficients in this new physics parameter space. The process uses the operator product expansion and effective field theory to derive and define the operators and coefficients. The results found are consistent with those found in Fleischer *et al.* and are in agreement with the SM at the (1-2)σ level. The impact of the currently unmeasured decay $B_c \to \tau\nu_\tau$, that the LHCb is planning, was also examined. It was shown that this measurement could remove ambiguity and improve the precision of the new physics Wilson coefficient constraints. Additionally, predictions for $B_c \to \tau\nu_\tau$ branching fraction are provided for scenarios where the new physics effects enter through pseudoscalar or left-handed vector interactions only.

Contents

1 Introduction

Over the last one and half century, since the original discovery of the electron by J.J. Thomson, many more particles and atoms have been discovered. Many particles initially assumed to be elementary, turned out to have a complex structure. Even protons and neutrons turned out to be composed of quarks. The Standard Model (SM) contains all particles considered to be fundamental point-like particles, which can be used to build up all other existing particles. The SM contains three generations of quarks and three generations of leptons. Additionally, there are four gauge boson types that allow interactions to occur between the quarks and leptons.

The Standard Model successfully explains the majority of particle physics aspects. However, several phenomena cannot be clarified by the SM. For example, it is not capable of resolving the matter-antimatter asymmetry in the universe, which according to the SM, should have been created in equal amounts [2]. Additionally, the SM is not able to define the nature of dark matter and dark energy. It is currently theorized that the Universe consists of 5% matter, 26% dark matter, and 69% dark energy. However, the SM does not contain possible dark matter candidates that would match the needed properties. Equivalently, attempts to define dark energy using the SM vacuum energy, results in a disagreement of 50–120 orders of magnitude with observations. This is also known as the cosmological constant problem [3]. Additionally, the SM accounts for all fundamental forces except for gravity and conflicts with the theory of general relativity [4]. Furthermore, the SM defines neutrinos as massless particles. This is in disagreement with neutrino oscillation experiments. The exact mass and nature of the neutrino masses are still unknown [5].

These shortcomings of the SM and several others have led to the search for physics beyond the SM. To this day, no experimental proof has yet been found that shows a disagreement with the SM beyond the set threshold of 5σ. However, strong hints of physics beyond the SM have been discovered. Experiments that look for this 'new physics' (NP) can mainly be divided into so called direct and indirect methods. Direct experiments look for new particles that are not in the SM. Indirect experiments do this largely by comparing the SM prediction to experimental measurements of for example branching fractions of certain decay modes. This includes the test of lepton flavour universality (LFU), which implies the three charged leptons of the SM are identical except for their mass. Consequently, the coupling between leptons and bosons should be identical, independent of lepton flavour [6]. Additionally, there is the quark sector of the SM, which is described by the Cabibbo-Kobayashi-Maskawa (CKM) matrix which characterizes the mixing between different quark flavours.

One particular particle that is used to explore the NP parameter space, is the B meson. A B meson is a composite particle that consists of a bottom quark paired with an up, down, charm, or strange quark. Particularly rare B meson decay modes are of interest. Many of which are also used to probe violation of LFU. Previously, physicists have already observed discrepancies between theoretical predictions and experimental measurements in the parameters known as $\mathcal{R}(D)$ and $\mathcal{R}(D^*)$. $\mathcal{R}(D)$ and $\mathcal{R}(D^*)$ are both defined by a ratio of the fraction of B meson decays to the $D^{(*)}$ meson and leptons. The Large Hadron Collider beauty experiment (LHCb) also examines decays involving the bottom (also called beauty) quark. Currently, the LHCb group of the Van Swinderen Institute in Groningen is planning to measure the decay of the B_c meson to a tau lepton and neutrino. Its branching fraction can be compared to its SM prediction to potentially give more information on the tension with the SM.

In this thesis we will follow the work of Fleischer *et al.* [1]. In this paper a method is presented to constraint coefficients corresponding to the NP parameter space. The method is applied to observables that are related to different (semi-) leptonic B meson decays containing $b \to u$ and $b \to c$ transitions. This thesis will reproduce the NP constraints for $b \to c$ transitions and extend this work by showing in more detail the potential impact of a $B_c \to \tau\nu_\tau$ measurement.

This thesis will first cover the basics of the standard model, including the CKM matrix (section 2.1). After this, the decay modes of the B meson relevant to this thesis will be elaborated (section 2.2), and a short summary of the LHCb experiment is given (section 2.3). Sections 2.4 and 2.5 explain the theoretical framework and context needed for the analysis of the NP coefficients. Afterward, we will first look at constraining the NP components of the short-distance parameters, known as Wilson coefficients, for $b \to c$ transitions (section 3). In this process $\mathcal{R}(D)$ and $\mathcal{R}(D^*)$ play a major role. Finally, the potential impact of a $B_c \to \tau\nu_\tau$ measurement on this NP parameter space will be determined (section 4). Constraining the short-distance parameters further could also contribute and give more insight into physics beyond the standard model.

2 Theoretical Background

2.1 The Standard Model

The goal of the Standard Model is to describe all phenomena in particle physics as a result of three of the four fundamental forces: the electromagnetic, weak, and strong force. Gravity is not taken into account. It defines the properties and interactions of a limited number of fundamental particles, defined as point-like particles. Some characteristics of these particles are their mass, charge, and spin. Half-integer spin particles are defined as fermions and those with integer spin as bosons. In the SM, there are two fermion families. The first is the quarks, which interact through strong interactions. The second is the leptons, which include the electron, muon, tau lepton, and neutrinos. The bosons include a spin-1 family, which are the force carriers of the SM. The spin-0 boson is the Higgs boson, which is involved in the mass of the fundamental particles. [7]

Electromagnetic interactions are mediated by the exchange of photons. Similarly, the weak interactions are mediated by the W^+, W^-, and Z^0 bosons, which are also spin-1 gauge bosons. The strong interactions are mediated by gluons, which are massless neutral bosons. In the SM strong interactions can be described by the theory of quantum chromodynamics (QCD). In this theory, gluons are coupled to colour charges. In total, there are three colour states for quarks, which all also have an anticolour. Gluons carry a combination of colour and anticolour, which results in eight unique possible colour states. [7]

Besides fundamental particles, the SM also includes bound states of quarks, named hadrons. There exist hundreds of different hadrons, of which the majority are unstable and decay by electromagnetic, weak, or strong interactions. Two common subgroups are baryons, which consist of 3 quarks and mesons, which consist of 2 quarks, a quark, and an antiquark. According to the QCD, composite particles like hadrons must have a zero colour charge. [8]

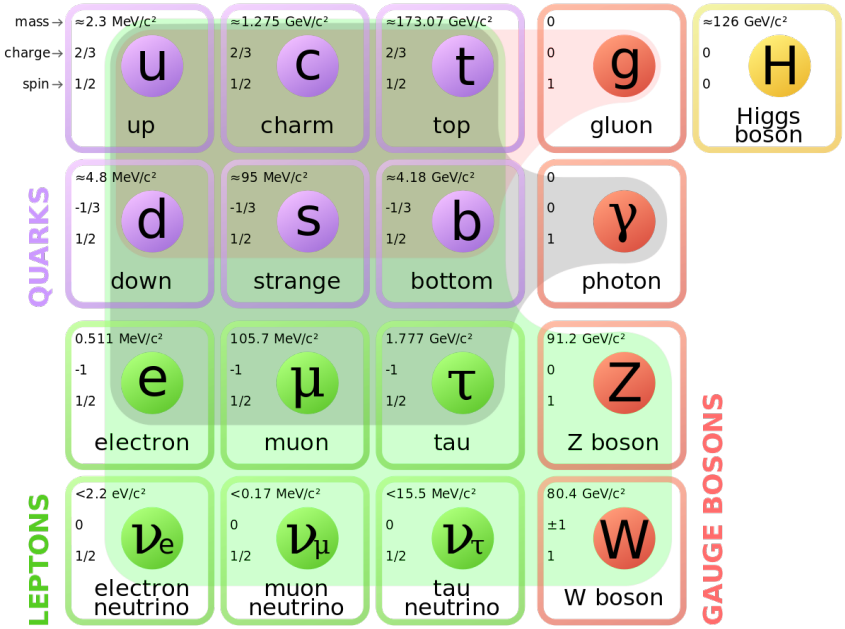

Figure 1: Elementary particles of the SM, consisting of 12 fermions and 5 bosons. The 3 quark generations are shown in purple. Also, the charged and neutral lepton make up 3 generations, shown in green. For both fermion families, corresponding anti-particles exist. In red, the gauge bosons are shown, which are responsible for interactions between fermions. The Higgs boson, shown in yellow, generates the mass of bosons. [5]

2.1.1 CKM Matrix

In contrast to electromagnetic interactions and QCD, weak interactions do mix quark flavours. The mixing between quarks is described by the Cabibbo–Kobayashi–Maskawa (CKM) Matrix (eq. (2.1)), which allows for the decay of the three quark generations by weak interactions.

$$\begin{bmatrix} d' \\ s' \\ b' \end{bmatrix} = \begin{bmatrix} V_{ud} & V_{us} & V_{ub} \\ V_{cd} & V_{cs} & V_{cb} \\ V_{td} & V_{ts} & V_{tb} \end{bmatrix} \begin{bmatrix} d \\ s \\ b \end{bmatrix} \tag{2.1}$$

Each element $V_{\alpha\beta}$ ($\alpha = u, c, t; \quad \beta = d, s, b$) is related to the probability of a transition from quark flavour β to α, with the probability being proportional to $|V_{\alpha\beta}|^2$ [7].

An important factor in branching fractions of decays involving $b \to c$ quark transitions, is the CKM matrix element $|V_{cb}|$. There are an inclusive and exclusive determinations of this value, which are not in full agreement with each other. The exclusive determination is dependent on certain decay processes, specifically particular B meson decays involving $b \to c$ quark transitions with leptons in the final state. The value is extracted from measurements of observables that include these decays. A external determination was computed using the $\bar{B} \to D\ell^-\bar{\nu}_\ell$ decay, giving the following value [1]:

$$|V_{cb}| = 0.03958 \pm 0.00117 \tag{2.2}$$

The inclusive determination instead is determined from a wide range of decays, namely all (semi-) leptonic B decays involving $b \to c$ quark transitions. The inclusive value of $|V_{cb}|$ is given by [9]:

$$|V_{cb}| = 0.04162^{+0.00026}_{-0.00080} \tag{2.3}$$

Both methods use different theoretical frameworks and calculation, which could partially explain the disagreement between the two determinations. The exclusive determinations are also more strongly model-dependent compared to inclusive determinations, which increases the probability of discrepancies in the results. Due to the exclusive determinations being dependent on specific decay modes with limited statistics, it is more likely statistical uncertainties corresponding to these modes are involved. On the contrary, inclusive determinations have larger statistics but can still be limited by for example the separation of signal from background contributions [9].

2.2 B meson decays

This thesis will analyse the impact of different B meson decays on the New Physics parameter space. Therefore it is important to understand how the different components and decays are defined. Each meson is composed of an equal number of quarks and antiquarks. In the case of the B meson, it consists of a bottom antiquark together with an up quark (B^+, charged B meson), down quark (B^0, neutral B meson), strange quark (B_s^0, strange B meson) or charm quark (B_c^+, charmed B meson). For each of these, a corresponding anti B meson exists as well. B mesons are of particular interest due to the sensitivity of their rare decay paths on NP effects and the CKM elements.

An example of this are the semileptonic $B \to D^* \ell \nu$ decays. Semileptonic implies that a hadron decays to form a different hadron and leptons. The $\bar{B} \to D^{(*)+} \tau^- \nu_\tau$ decay is shown in fig. 2 (right-hand side). The down antiquark does not interact in the decay and is therefore labelled a spectator quark. The decay is sensitive to the CKM element $|V_{cb}|$, due to the vertex between the bottom and charm quark. Several more $B \to D^* \ell \nu_\ell$ are possible and used in this thesis. Whenever the specific state of the B or D meson is left unspecified, e.g. $B \to D^* \tau \bar{\nu}_\tau$, a combination of transitions containing a D^* meson in the final state is implied.

The final focus of the thesis will be on the tauonic decay of the charmed B meson B_c:

$$B_c^+ \to \tau^+ \nu_\tau, \qquad B_c^- \to \tau^- \bar{\nu}_\tau \tag{2.4}$$

This decay is purely leptonic, meaning the final state contains only leptons. The Feynman diagram of the B_c^+ decay is given in fig. 2 (left-hand side). The decay is theoretically well understood because the decay can be split into a quark initial state (QCD) and a lepton final state, independent of QCD. The sensitivity to QCD shows through the B_c decay constant. This decay is also sensitive to weak interactions, due to the flavour asymmetry of the bottom and charm quark, making annihilation through a gluon or photon impossible. [10]

All discussed decays in this thesis are purely or semileptonic decays involving a $b \to c$ transition. Consequently, they are all sensitive to $|V_{cb}|$ and the same set of coefficients.

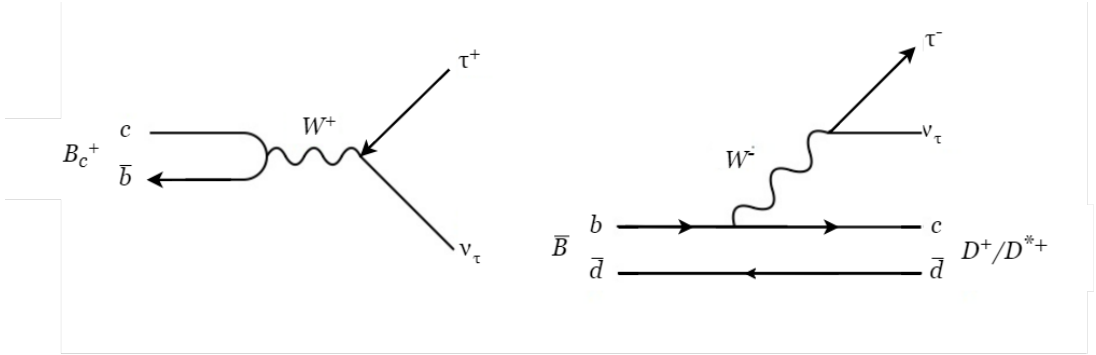

Figure 2: The tauonic decay of B_c^+ (left) and a semileptonic decay of B^0 (right), both containing a $b \to c\tau\nu_\tau$ transition through the exchange of a W boson.

2.2.1 Disagreement of $\mathcal{R}(D)$ and $\mathcal{R}(D^*)$ SM values and measurements

Besides physical phenomena that cannot be explained by the SM, the first hints towards finding physics beyond the SM are experimental results that are in tension with the SM. An example of this is certain B meson decays. This is accomplished by analysing and comparing the decay probability of different purely or semileptonic decays for which only the flavour of the lepton differs. The probability of a certain decay mode occurring is given by the branching fraction $\mathcal{B}$, which is the fraction of decays to the final state of interest compared to all possible final states [7]. Comparing the experimental ratio between the branching fractions with the SM prediction could reveal a disagreement. If there is sufficient statistical certainty, this could prove the existence of physics beyond the SM. One particular set of decays for which these measurements are performed are: $\bar{B} \to D^{(*)}\tau^-\bar{\nu}_\tau$ and $\bar{B} \to D\ell'^-\bar{\nu}_{\ell'}$, where $\ell' = e, \mu$. The ratio between the branching fractions of these decays are labelled $\mathcal{R}(D)$ and $\mathcal{R}(D^*)$. The equations of $\mathcal{R}(D)$ and $\mathcal{R}(D^*)$ are independent of $|V_{cb}|$, because the CKM element cancels in the fractions.

$$\mathcal{R}(D) = \frac{\mathcal{B}(\bar{B} \to D\tau^-\bar{\nu}_\tau)}{\mathcal{B}(\bar{B} \to D\ell'^-\bar{\nu}_{\ell'})} \tag{2.5}$$

$$\mathcal{R}(D^*) = \frac{\mathcal{B}(\bar{B} \to D^*\tau^-\bar{\nu}_\tau)}{\mathcal{B}(\bar{B} \to D^*\ell'^-\bar{\nu}_{\ell'})} \tag{2.6}$$

D is a pseudoscalar meson state and D^* is a vector meson state. The branching fractions included here are the combined average of the $\bar{B}^0 \to D^{(*)+}\ell^-\bar{\nu}_\ell$ and $B^- \to \bar{D}^{(*)0}\ell^-\bar{\nu}_\ell$ decays. These ratios have been measured by LHCb, BaBar and Belle [11] and presented as [12]:

$$\mathcal{R}(D) = 0.340 \pm 0.030, \quad \mathcal{R}(D^*) = 0.295 \pm 0.014 \tag{2.7}$$

These measurements have a 3σ discrepancy with SM. The theoretical SM values have been estimated at [1]:

$$\mathcal{R}(D)|_{SM} = 0.300 \pm 0.006, \quad \mathcal{R}(D^*)|_{SM} = 0.253 \pm 0.005 \tag{2.8}$$

The Heavy Flavour Lattice Averaging Group (HFLAV) has collected and combined measurements from different collaborations including LHCb, Belle, and BaBar (see fig. 3). The weighted average of these results shows a 3.2σ disagreement with SM prediction [13]. The $B_c \to \tau\nu_\tau$ decay shares the dependency on the same NP coefficients as $\mathcal{R}(D)$ and $\mathcal{R}(D^*)$. Consequently, this tension with the SM, is likely to be present in $B_c \to \tau\nu_\tau$ as well.

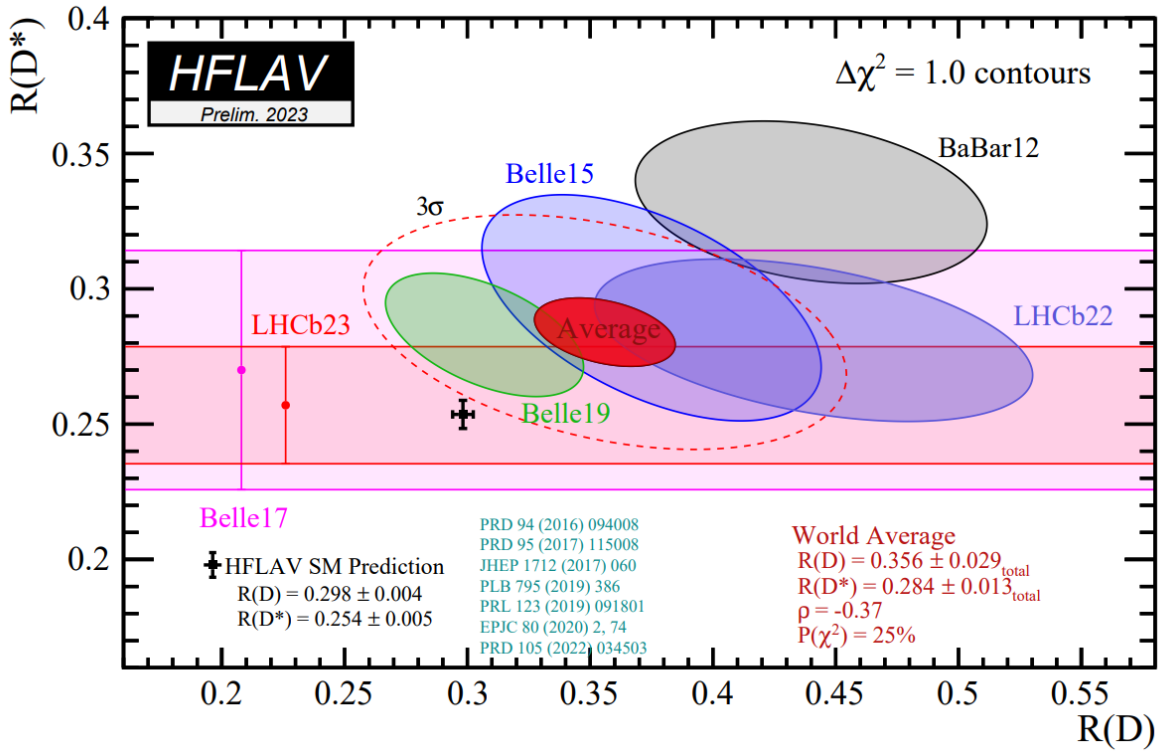

Figure 3: Combination of measurements of $\mathcal{R}(D)$ and $\mathcal{R}(D^*)$ from LHCb, BaBar and Belle to provide a preliminary HFLAV average of $\mathcal{R}(D)$ and $\mathcal{R}(D^*)$. The contours shown correspond to $\Delta\chi^2 = 1.0$ or 1σ [13].

2.3 LHC and the LHCb experiment

Despite the main focus of this thesis being a theoretical analysis of several B meson decays, it is connected to the experiments performed at the Large Hadron Collider (LHC) near Geneva, Switzerland, specifically the Large Hadron Collider beauty (LHCb) experiment. LHCb is one of the four main detectors, the others are ATLAS, CMS, and ALICE.

LHC is the largest particle accelerator on earth, with a 27-kilometer ring. It was built by the European Organization of Nuclear Research (CERN) and finished in 2008. However, it has undergone several upgrades over the last decade. It functions by accelerating and colliding protons and heavy ions at high speeds. One of the most notable results of the LHC is the discovery of the Higgs boson in 2012 [14].

The LHCb experiment is focused on measuring decays involving the bottom (beauty) quark. Its main goal is to explore physics beyond the SM by examining b-hadron decays and CP-violation. This could try to help resolve the matter-antimatter asymmetry problem. Despite LHCb being originally designed for heavy-flavour physics, it is also able to do measurements for electroweak and heavy ion physics [15]. Some LHCb measurements are focused on measuring rare decay modes of B mesons. Their rarity implies they are strongly suppressed in the SM, which increases the probability of discovering NP effect, due to their relatively higher deviation from the SM prediction. One such example is the decay $B^0 \to K^{*0}\mu^+\mu^-$, for which the found decay rate and angle distribution of decay products is in disagreement with the SM prediction [16].

Currently, the LHCb group that is located at the Van Swinderen Institute in Groningen is planning to measure the $B_c \to \tau\nu_\tau$ decay. This measurement could help probe the NP parameter space through its sensitivity of NP effects coming from certain interactions. More details on this and the potential impact of the measurement are provided in section 4.

2.4 From Full Theory to Effective Field Theory

The full SM theory of weak interactions can get very complex and computationally challenging. Instead one can employ a theoretical framework known as Effective Field Theory (EFT), which makes it possible to describe weak interactions at certain energy scales without knowing the exact underlying theory at higher energies. This makes EFT a useful tool to examine and understand experimental results.

A popular EFT framework is the Standard Model effective field theory (SMEFT). Due to a lack of evidence for NP from colliders, it can be assumed with a high probability that NP particles will have a mass significantly larger than the weak scale. SMEFT also helps to resolve issues with the SM, like the hierarchy problem, dark matter, and neutrino masses. This has led to the search for NP at the TeV energy scale. The LHC has also led attraction to SMEFT. [5, 17]

Weak transitions can be analysed as occurring through a point interaction. This was first described by Fermi in 1933 for the nuclear β decay $n \to p^+ e^- \bar{\nu}_e$ [18]. B meson decays can also be described as a four-point fermion interaction and constitute a low-energy effective theory. The formalism used to describe such interactions is the operator product expansion (OPE). OPE makes the computation of weak interactions possible by removing the dependence on higher energy scales.

2.4.1 Effective Hamiltonian of a Non-Leptonic Transition using OPE

As an example $c\bar{s} \to u\bar{d}$ transitions will be used. Figure 4 shows the Feynman diagram of the non-leptonic decay for the full SM theory and the weak effective theory. The latter uses a local 4-fermion interaction, which is formed by contracting the propagation of the W boson, thereby removing the W boson dependence. This process will be further explained and derived in this section. The decay amplitude corresponding to the full SM theory can be constructed from the Feynman diagram. The first and last components in the equation of the decay amplitude (eq. (2.9)) represent the initial and final state respectively; the second and fourth components represent the two vertices, and the middle component represents the propagator. [19]

$$A = (\bar{s}_\beta c_\alpha)_{\text{V-A}} \times \frac{g_{\text{EW}} V_{cs}^*}{2\sqrt{2}} \delta_{\alpha\beta} \times \frac{1}{k^2 - m_W^2} \left(g^{\mu\nu} - \frac{k^\mu k^\nu}{m_W^2} \right) \times \frac{g_{\text{EW}} V_{ud}}{2\sqrt{2}} \delta_{\gamma\delta} \times (\bar{u}_\delta d_\gamma)_{\text{V-A}} \tag{2.9}$$

Where α, β, γ, and δ are the colour indices of the quarks. μ and ν are Lorentz indices, specifying the space-time dimension. g_{EW} is electroweak coupling constant. $g^{\mu\nu}$ is the metric tensor. k is the momentum transferred by the W boson. Finally, V-A stands for the subtraction of an axial vector from a vector, and represents the chiral structure of the interaction. The components $(\bar{q}p)_{\text{V-A}}$ can be expressed in terms of gamma matrices γ_μ as follows:

$$(\bar{q}p)_{\text{V-A}} \equiv \bar{q}\gamma_\mu(1 - \gamma_5)p \tag{2.10}$$

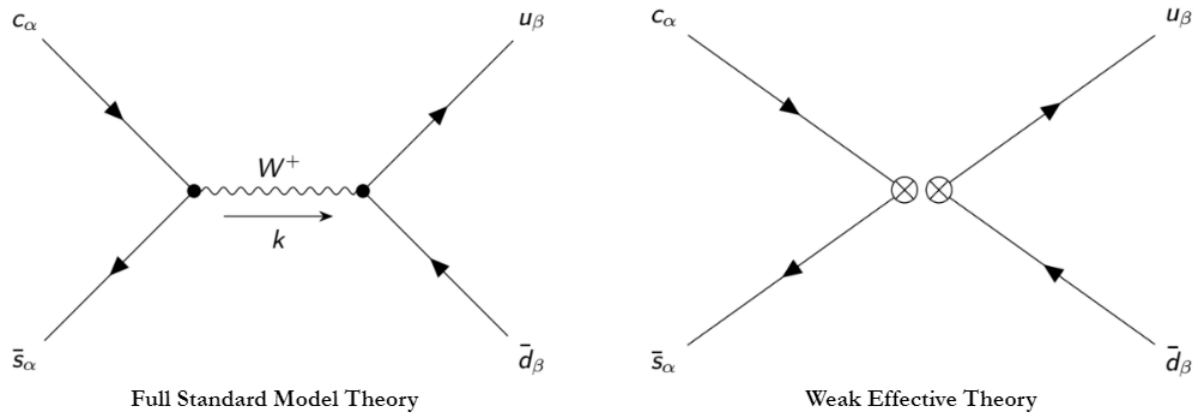

Figure 4: The Feynman diagram of a simply non-leptonic decay according to the full SM theory (left). The interaction occurs through exchange of a W boson. Based on the weak effective theory, the interaction can be simplified to a local 4-fermion interaction (right). [19]

.

Based on eq. (2.9), the Hamiltonian $\mathcal{H}$ of $c\bar{s} \to u\bar{d}$ transitions can be constructed equivalently [20]:

$$\mathcal{H} = \frac{g_{\text{EW}}^2}{8} V_{cs}^* V_{ud} (\bar{s}_\alpha c_\alpha)_{\text{V-A}} (\bar{u}_\beta d_\beta)_{\text{V-A}} \times \frac{1}{k^2 - m_W^2} \left(g^{\mu\nu} - \frac{k^\mu k^\nu}{m_W^2} \right) \tag{2.11}$$

Due to the fermions and boson involved in the interaction, the interactions can be separated into two different energy scales. The average energy scale is on the same scale as the b quark mass ($m_b = 4.18 \pm 0.03$ GeV/c^2), compared to ($m_W = 80.385 \pm 0.015$ GeV/c^2) mass of the W boson. [21] Consequently, the propagator term eq. (2.11) can be simplified on the basis that the momentum k is on the same order as m_q, using a Taylor series expansion to first order:

$$\frac{1}{k^2 - m_W^2} \left(g^{\mu\nu} - \frac{k^\mu k^\nu}{m_W^2} \right) \xrightarrow{k \ll m_W} \frac{g^{\mu\nu}}{m_W^2} + \mathcal{O}\left(\frac{k^2}{m_W^2} \right) \tag{2.12}$$

As a result, the expression has become independent of the W boson and larger energy scales. Now the full SM Hamiltonian can be expressed in terms of the Fermi constant ($G_F = \sqrt{2} g_{\text{EW}}^2 / 8 m_W^2$), to obtain the following expression:

$$\mathcal{H} = \frac{G_F}{\sqrt{2}} V_{cs}^* V_{ud} (\bar{s}_\alpha c_\alpha)_{\text{V-A}} (\bar{u}_\beta d_\beta)_{\text{V-A}} + \mathcal{O}\left(\frac{k^2}{m_W^2} \right) \tag{2.13}$$

Equation (2.13) can be rewritten in terms corresponding to the Operator Product Expansion (OPE). Substituting the operator $\mathcal{O}_2 = (\bar{s}_\alpha c_\alpha)_{\text{V-A}} (\bar{u}_\beta d_\beta)_{\text{V-A}}$ and Wilson coefficient $C_2 = 1$, and removing the higher orders, results in the following effective Hamiltonian [22]:

$$\mathcal{H}_{\text{eff}} = \frac{G_F}{\sqrt{2}} V_{cs}^* V_{ud} C_2 \mathcal{O}_2 \tag{2.14}$$

Figure 5 shows different contributions to $\mathcal{O}_2$ that occur besides the leading order diagram (fig. 4). This includes higher-order QCD effects like a vertex correction (fig. 5a), where a gluon is exchanged in the initial state. Additionally, a colour-neutral gluon exchange can occur between the initial and final state (fig. 5b). However, there is also a possibility a coloured gluon is exchanged. In this case a gluon mixes the colour indices of the initial and final state, as is shown in fig. 5c.

Consequently, a new operator has to be added, corresponding to a different colour structure. The new operator is defined as: $\mathcal{O}_1 = (\bar{s}_\beta c_\alpha)_{\text{V-A}}(\bar{u}_\alpha d_\beta)_{\text{V-A}}$, and has a corresponding Wilson coefficient C_1. The final possible gluon exchange is shown in fig. 5d. This diagram contributes to both operators ($\mathcal{O}_1$, $\mathcal{O}_2$) and coefficients (C_1, C_2). The resulting effective Hamiltonian is given by [22]:

$$\mathcal{H}_{\text{eff}} = \frac{G_F}{\sqrt{2}} V_{cs}^* V_{ud} (C_1 \mathcal{O}_1 + C_2 \mathcal{O}_2) \tag{2.15}$$

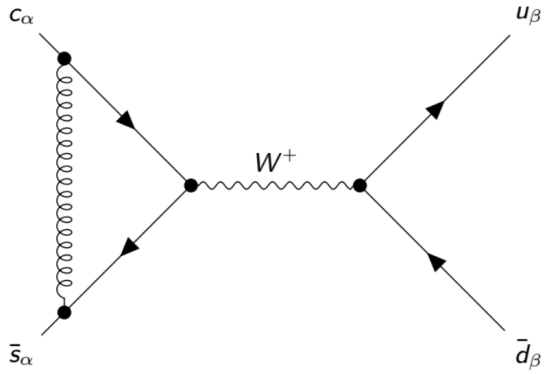

(a) Gluon is exchanged in the initial state, with no change to colour structure. Contributes to the $\mathcal{O}_2$ operator.

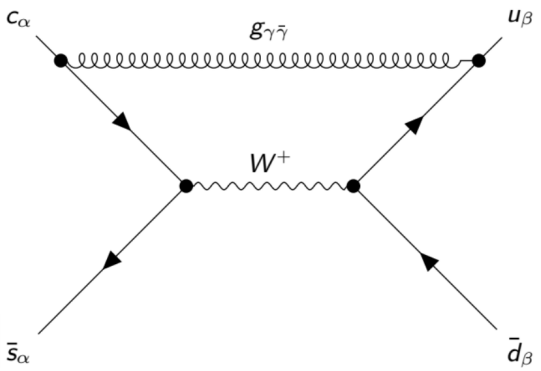

(b) Colour-neutral gluon exchange, with no change to colour structure. Contributes to the $\mathcal{O}_2$ operator.

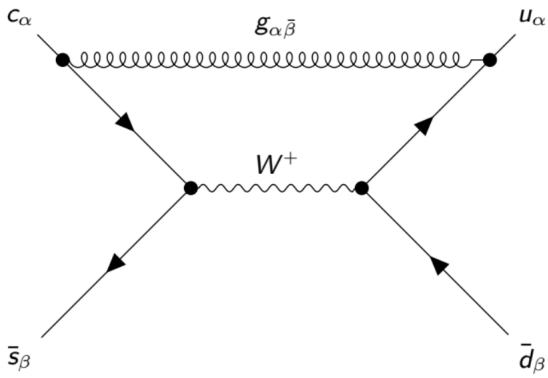

(c) Coloured gluon exchange, colour indices are mixed, resulting in a new colour structure. Contributes to the $\mathcal{O}_1$ operator.

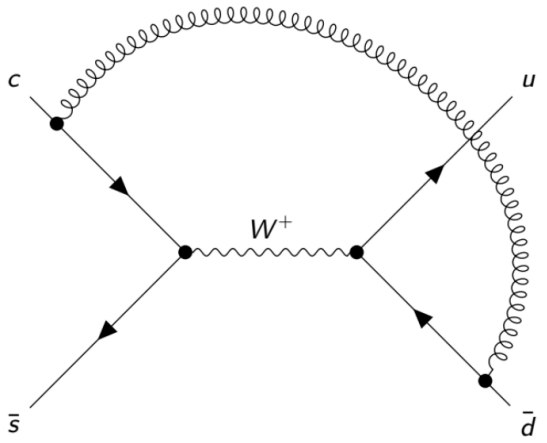

(d) Gluon exchange with the possibility of changing the colour structure. Contributes to both the $\mathcal{O}_1$ and $\mathcal{O}_2$ operator.

Figure 5: Next to Leading Order QCD diagrams of a local 4-fermion interaction [19].

The operators discussed so far correspond to current-current diagrams. Other operators exist as well, for example, operators corresponding to QCD and electroweak penguin diagrams. Besides the suppression that occurs due to additional gluon exchange, these penguin diagrams have an extra suppression by a factor of $\alpha_s/4\pi$ and $\alpha_{\text{QED}}/4\pi$ respectively, at the $\mu = m_b$ energy scale [20]. However, in this thesis, the focus will lie on current-current operators and the others will not be further discussed. Higher-dimensional operators are suppressed by powers of $1/m_W$ and will also be neglected in the following derivation and analysis.

For any weak decay interaction, the effective Hamiltonian can be similarly constructed as eq. (2.15), and will take the form of:

$$\mathcal{H}_{\text{eff}} = \frac{G_F}{\sqrt{2}} V_{pq}^* V_{ab} \sum_j C_j \mathcal{O}_j \tag{2.16}$$

In OPE, the operators $\mathcal{O}_j$ and Wilson coefficients C_j are related to long- and short-distance physics respectively. Where long-distance physics is related to QCD effects below the energy scale μ, and short-distance physics to energies above μ. Subsequently allowing for the separation of low and high energies [20]. The values of the Wilson coefficients solely depend on hard scattering processes. As a consequence, the coefficients are universal. While the effective Hamiltonian is independent of the energy scale μ, both $\mathcal{O}_j$ and C_j are dependent on μ, meaning their dependence cancels. μ allows for the separation of the long- and short-distance regimes [22]. Consequently, OPE facilitates the computation of weak decays that would otherwise be too computationally challenging. Due to the Wilson coefficients being universal, results of the effective theory at low energies can be matched to the full theory and vice versa computations of the full theory at high energies can be related to a prediction of the effective theory at lower energies [20].

The example shown in this section covered a non-leptonic decay. However, it can also be applied to semi- and purely leptonic decays. In these cases, the final state in the operators $\mathcal{O}_j$ can often be replaced by $(\bar{\ell}\ell)_V$ or $(\bar{\ell}\ell)_A$.

2.4.2 Search for BSM using OPE

New Physics can take shape as undiscovered particles or interactions that contribute to these four-fermion interactions. Having different masses or coupling strengths than the SM predicts, leads to new contributions of the Wilson coefficients.

OPE is a useful method to search for physics beyond the SM. In this case, the Wilson coefficients are split up into a SM and a NP contribution. It is possible to compute the SM contribution C_j^{SM} to high precision, leaving the NP contributions C_j^{NP} the only unknowns.

$$\mathcal{H}_{\text{eff}} = \frac{G_F}{\sqrt{2}} V_{pq}^* V_{ab} \sum_j \left(C_j^{\text{SM}} + C_j^{\text{NP}}\right) \mathcal{O}_j \tag{2.17}$$

Based on experimental data of e.g. branching fraction and ratios, NP Wilson coefficients can be constrained using a model-independent approach. However, this method also has its downsides. Depending on which interaction is being examined, there are likely many different Wilson coefficients, leading to too many degrees of freedom. Consequently, one needs to make a selection of which operators and coefficients are included in the analysis, making it increasingly difficult to determine the significance of different components.

2.5 Theoretical Framework

In this thesis, we will look at purely and semileptonic decays of the B meson involving $b \to c$ transitions. Part of the reason these particular decays are of interest is the insight they give into the potential violation of LFU. Based on experimental results of the semi-leptonic $B \to D^{(*)}\ell\bar{\nu}_\ell$ transitions, constraints can be put on the NP contributions to the short-distance Wilson coefficients, related to their corresponding operators (section 3). This is done using the same method as presented by Fleischer *et al.* [1] (section 2.5). The results from the relevant effective Hamiltonian at the low energy scale $\mu = m_b$ are connected to high energies at 1 TeV through the proper renormalisation group evolution, presented in section 2.5.1. Additionally, we will examine how the planned measurement of the $B_c \to \tau\nu$ decay could potentially help further constrain these coefficients.

For $b \to c\tau\bar{\nu}_\ell$ transitions at the lowest dimension, the general effective Hamiltonian is given by eq. (2.18) (assuming neutrinos are left-handed). Unlike the current-current operators used in section 2.4 to define the effective Hamiltonian of a non-leptonic decay, specific vector, (pseudo-) scalar, and tensor operators are used for these (semi-)leptonic transitions. These are all the possible four-fermion operators for this transition, at the lowest dimension, which results in the following Hamiltonian:

$$\mathcal{H}^c_{\text{eff}} = \frac{G_{\text{F}}}{\sqrt{2}} V_{cb} \left[\tilde{C}^{c,\ell}_{V_L} \mathcal{O}^{c,\ell}_{V_L} + \tilde{C}^{c,\ell}_{V_R} \mathcal{O}^{c,\ell}_{V_R} + \tilde{C}^{c,\ell}_{S} \mathcal{O}^{c,\ell}_{S} + \tilde{C}^{c,\ell}_{P} \mathcal{O}^{c,\ell}_{P} + \tilde{C}^{c,\ell}_{T} \mathcal{O}^{c,\ell}_{T} \right] + \text{ h.c.} \tag{2.18}$$

Where c represents the charm quark, and ℓ the lepton flavour $\ell = e, \mu, \tau$. $\tilde{C}^{q,\ell}_a$ are the Wilson coefficients and $\mathcal{O}^{q,\ell}_a$ the operators. Where the subscript a can represent left-handed vector V_L, right-handed vector V_R, scalar S, pseudo-scalar P or the tensor T interactions. In case LFU is violated, these Wilson coefficients will be different for the three different lepton flavours. The Wilson coefficients consist of a SM and a potential NP part:

$$\tilde{C}^{q,\ell}_a = C^{(\text{SM})q,\ell}_a + C^{q,\ell}_a \tag{2.19}$$

Where $a = V_L, V_R, S, P, T$. The SM components are:

$$C^{(\text{SM})q,\ell}_{V_L} = 1, \qquad C^{(\text{SM})q,\ell}_{V_R} = C^{(\text{SM})q,\ell}_{S} = C^{(\text{SM})q,\ell}_{P} = C^{(\text{SM})q,\ell}_{T} = 0 \tag{2.20}$$

So $C^{(\text{SM})q,\ell}_a$ for $a = V_R, S, P, T$ are only dependent by their NP component. [1]

For $b \to c\tau\bar{\nu}_\ell$ transitions, the operators can be defined using the same formalism as discussed in section 2.4.1, representing the initial, quarks fields state and final, lepton fields state [1, 23].

$$\mathcal{O}^{c,\ell}_{V_L} = (\bar{c}\gamma^\mu P_L b)\,(\bar{\tau}\gamma_\mu P_L \nu_\ell) \tag{2.21}$$
$$\mathcal{O}^{c,\ell}_{V_R} = (\bar{c}\gamma^\mu P_R b)\,(\bar{\tau}\gamma_\mu P_L \nu_\ell) \tag{2.22}$$
$$\mathcal{O}^{c,\ell}_{S} = (\bar{c} b)\,(\bar{\tau} P_L \nu_\ell) \tag{2.23}$$
$$\mathcal{O}^{c,\ell}_{P} = (\bar{c}\gamma_5 b)\,(\bar{\tau} P_L \nu_\ell) \tag{2.24}$$
$$\mathcal{O}^{c,\ell}_{T} = (\bar{c}\sigma^{\mu\nu} P_L b)\,(\bar{\tau}\sigma_{\mu\nu} P_L \nu_\ell) \tag{2.25}$$

Where γ^μ represents four 4-dimensional gamma matrices, also known as Dirac matrices. $P_{L,R} = 1 \mp \gamma_5$, with γ_5 being a gamma matrix used to separate left and right chirality. μ and ν are

Lorentz indices, defining the spacetime dimension.

In the process of constraining the Wilson Coefficients, each lepton flavour should be analysed. To simplify this, three possible relations between the electron C_a^e and muon C_a^μ coefficients are applied. To make the analysis model-independent, C_a^e being smaller, equal, and greater than C_a^μ are considered. To be consistent with Fleischer *et al.*, the ratio:

$$C_a^e = f_\mu^e C_a^\mu \tag{2.26}$$

between C_a^e and C_μ^e is chosen to take the values: $f_\mu^e = 0.1, 1, 10$.

2.5.1 Evolution of NP Wilson Coefficients from the Low to High Energy Scale

The effective Hamiltonian (eq. (2.18)) and subsequent branching fractions are given for the low energy scale $\mu = m_b$. The resulting Wilson coefficient constraints can be connected to the high energy scale $\mu = 1$ TeV through the renormalisation group equation presented in eq. (2.27) [24]. This will also facilitate the comparison to the results of Fleischer *et al.*, which are presented for $\mu = 1$ TeV.

$$\begin{pmatrix} C_{V_L}^{q,\ell}(m_b) \\ C_{V_R}^{q}(m_b) \\ C_{S}^{q,}(m_b) \\ C_{P}^{q,\ell}(m_b) \\ C_{T}^{q,\ell}(m_b) \end{pmatrix} \simeq \begin{pmatrix} 1 & 0 & 0 & 0 & 0 \\ 0 & 1 & 0 & 0 & 0 \\ 0 & 0 & 1.71 & 0 & -0.27 \\ 0 & 0 & 0 & 1.71 & 0.27 \\ 0 & 0 & 0 & 0 & 0.84 \end{pmatrix} \begin{pmatrix} C_{V_L}^{q,\ell}(1\text{TeV}) \\ C_{V_R}^{q}(1\text{TeV}) \\ C_{S}^{q,\ell}(1\text{TeV}) \\ C_{P}^{q,\ell}(1\text{TeV}) \\ C_{T}^{q,\ell}(1\text{TeV}). \end{pmatrix}. \tag{2.27}$$

3 $b \to c$ Transitions — Constraining Wilson Coefficients

Fleischer *et al.*, 2021 [1] have computed and analysed the constraints on Wilson Coefficients corresponding to $b \to c$ transitions, with the goal of estimating the $|V_{cb}|$ element. Specifically, the semileptonic B decays $B \to D\tau\bar{\nu}_\tau$ and $B \to D^*\ell\bar{\nu}_\ell$ are used. In this section we follow the derivation and discussion from Fleischer *et al.*, which is summarised below. I have reproduced the figures and numerical values and compare them to the results published in [1]. In section 4, these constraints will be used in combination with the (inclusive and exclusive) determination of $|V_{cb}|$ to analyse how potential measurements of $B_c \to \tau\nu_\tau$ can further constraint the NP coefficients.

To successfully constrain NP Wilson coefficients, observables that have been experimentally determined are required. The ratio of branching fractions $\mathcal{R}(D)$ and $\mathcal{R}(D^*)$, presented in eqs. (2.5) and (2.6), fulfil this requirement. In the upcoming analysis, the NP effects of the heavy and light lepton generation will be evaluated separately. Therefore, to equate the $\mathcal{R}(D^{(*)}$ ratio to its experimental result, the expressions of the heavy and light generations have to be multiplied. If NP comes through the light generations, the ratio evaluated for τ, will become 1, and vice versa. Furthermore, eq. (3.1) allows for a relation between $C_a^{c,\tau}$ and $C_a^{c,\mu}, C_a^{c,e}$ to be established.

$$\frac{\mathcal{R}(D^{(*)})}{\mathcal{R}(D^{(*)})^{SM}} = \frac{\mathcal{R}(D^{(*)})}{\mathcal{R}(D^{(*)})^{SM}}\bigg|_{e,\mu} \frac{\mathcal{R}(D^{(*)})}{\mathcal{R}(D^{(*)})^{SM}}\bigg|_{\tau} \tag{3.1}$$

Based on the experimental values presented in eqs. (2.7) and (2.8), the following values and uncertainties are computed:

$$\frac{\mathcal{R}(D^*)}{\mathcal{R}(D^*)^{SM}} = 1.17 \pm 0.06, \qquad \frac{\mathcal{R}(D)}{\mathcal{R}(D)^{SM}} = 1.1 \pm 0.1 \tag{3.2}$$

Furthermore, the polarization ratio (eq. (3.3)) can be used for NP Wilson coefficients constraints, for semileptonic decays that decay to a final state containing a D^* meson. The ratio is expressed in terms of the decay width of the B meson decay to the left-handed vector meson state D_L^* and the unpolarized state D^*.

$$F_L(D^*) = \frac{\Gamma(B \to D_L^* \tau\bar{\nu}_\tau)}{\Gamma(B \to D^* \tau\bar{\nu}_\tau)} \tag{3.3}$$

Also for this observable a SM estimate [1] and experimental results by Belle [25] are available. The values have a disagreement of 1.6σ.

$$F_L(D^*)|_{SM} = 0.458 \pm 0.004, \quad F_L(D^*) = 0.60 \pm 0.08 \pm 0.04 = 0.60 \pm 0.09 \tag{3.4}$$

The final observable used to determine the constraints is the ratio represented in eq. (3.5). Which can be used to analyse the LFU between electrons and muons. Subsequently, it can be used to constrain the coefficients corresponding to ℓ'.

$$\mathcal{R}_\mu^e(D^*) = \frac{\mathcal{B}(B^0 \to D^{*-} e^+ \nu_e)}{\mathcal{B}(B^0 \to D^{*-} \mu^+ \nu_\mu)} \tag{3.5}$$

The SM estimate [1] and the experimental results by Belle [26] are:

$$\mathcal{R}_\mu^e(D^*)|_{\text{SM}} = 1.0045(1), \quad \mathcal{R}_\mu^e(D^*) = 1.01 \pm 0.01 \pm 0.03 = 1.01 \pm 0.04 \tag{3.6}$$

In sections 3.1 to 3.4, ratios between $\mathcal{R}(D)$, $\mathcal{R}(D^*)$, $F_L(D^*)$, $\mathcal{R}_\mu^e(D^*)$ and their SM counterparts, will be used to constrain the NP Wilson coefficients for pseudoscalar, scalar, vector, and tensor

interactions. Each will be considered separately, assuming no contribution from other interaction types. In reality, a combination of different interactions is likely to contribute to the NP effects. Furthermore, the method will only reveal the interactions that are allowed, without revealing anything about the underlying theory.

Fleischer *et al.* [1] provides expressions, showing the dependence of these observables on the NP Wilson coefficients at $\mu = m_b$. For every interaction type, the relevant components will be extracted from these expressions, and the resulting equations will be presented in each section. Subsequently, the constraints will be determined by relating these equations to the experimental measurements and theoretical SM estimates of the observables. The constraints will be evaluated and presented for the three different scenarios concerning the relation between C_a^e and C_μ^e (eq. (2.26)).

3.1 Constraints on Pseudo-scalar Wilson Coefficients

The first variables to be constrained are the pseudo-scalar Wilson coefficients. The ratio between $\mathcal{R}(D)$ and $\mathcal{R}(D^*)$ and their SM prediction are evaluated for two different scenarios: heavy generation, τ leptons contribute the NP; or light generations, electrons, and muons contribute the NP. Additionally, $F_L(D^*)$ will only be related to the τ coefficients, due to it being solely defined by semileptonic $b \to c\ell\bar{\nu}_\ell$ transitions containing τ in the final state (eq. (3.3)). The following dependencies on the pseudoscalar coefficients for the τ lepton are found from derivation of expressions provided by Fleischer *et al.* [1]:

$$\mathcal{R}(D^*)/\mathcal{R}(D^*)^{SM}|_\tau = 1.00 + 0.11Re[C_P^{c,\tau *}] + 0.034|C_P^{c,\tau}|^2 \tag{3.7}$$

$$\mathcal{R}(D)/\mathcal{R}(D)^{SM}|_\tau = 1.00 \tag{3.8}$$

$$F_L(D^*) = \left(\mathcal{R}(D^*)^{SM}/\mathcal{R}(D^*)|_\tau\right)\left(0.46 + 0.11Re[C_P^{c,\tau *}] + 0.034|C_P^{c,\tau}|^2\right) \tag{3.9}$$

Where an $*$ in the superscript of $C_a^{c,\ell}$ indicates the complex conjugate. Recall that $C_a^{c,\ell}$ represents only the NP contribution to the Wilson coefficients. It can be seen that in this case for the $B \to D\tau^-\bar{\nu}_\tau$ transition, there is no dependence on NP pseudoscalar coefficient, i.e. any deviation of $\mathcal{R}(D)$ from the SM cannot be explained by pseudoscalar NP effects.

Similarly, we find the expressions for the light generations. For both cases, the electron and muon components are separately given.

$$\mathcal{R}(D^*)/\mathcal{R}(D^*)^{SM}|_{e,\mu} = \frac{1}{G_\mu^{D^*} + G_e^{D^*}} \tag{3.10}$$

With

$$G_\mu^{D^*} = 0.499 + 0.009Re[C_P^{c,\mu *}] + 0.025|C_P^{c,\mu}|^2 \tag{3.11}$$

$$G_e^{D^*} = 0.501 + 4.50 \times 10^{-5}Re[C_P^{c,e *}] + 0.026|C_P^{c,e}|^2 \tag{3.12}$$

And the effects on $\mathcal{R}(D)$:

$$\mathcal{R}(D)/\mathcal{R}(D)^{\mathrm{SM}}|_{e,\mu} = \frac{1}{G_\mu^{D} + G_e^{D}} = 1.00 \tag{3.13}$$

Like the evaluation for τ leptons, $\mathcal{R}(D)/\mathcal{R}(D)^{\mathrm{SM}}$ shows no NP pseudoscalar dependence for electrons and muons either.

Due to $F_L(D^*)$ being only dependent on $C_P^{c,\tau}$, the bounds imposed by the experimental data (eq. (3.4)) are straightforwardly determined. The resulting constraints on $C_P^{c,\tau}$ at $\mu = 1$ TeV are: $(-3.83, -2.34)$ and $(0.44, 1.94)$. The connection from $\mu = m_b$ to $\mu = 1$ TeV is made by eq. (2.27), which simplifies to $C_P^{c,\ell}(m_b) = 1.71 C_P^{c,\ell}(1\text{TeV})$ for the current evaluated circumstance. These bounds are represented by the blue rectangular area in fig. 6. Likewise, the allowed regions in the $C_P^{c,\tau}$- $C_P^{c,\mu}$ plane can be determined using eq. (3.1). These are shown as blue, red, and green bands in fig. 6, where the width of the bands is directly related to the uncertainty in the observable. Additionally, it can be observed that the computed allowed regions are in disagreement with the SM at 1σ.

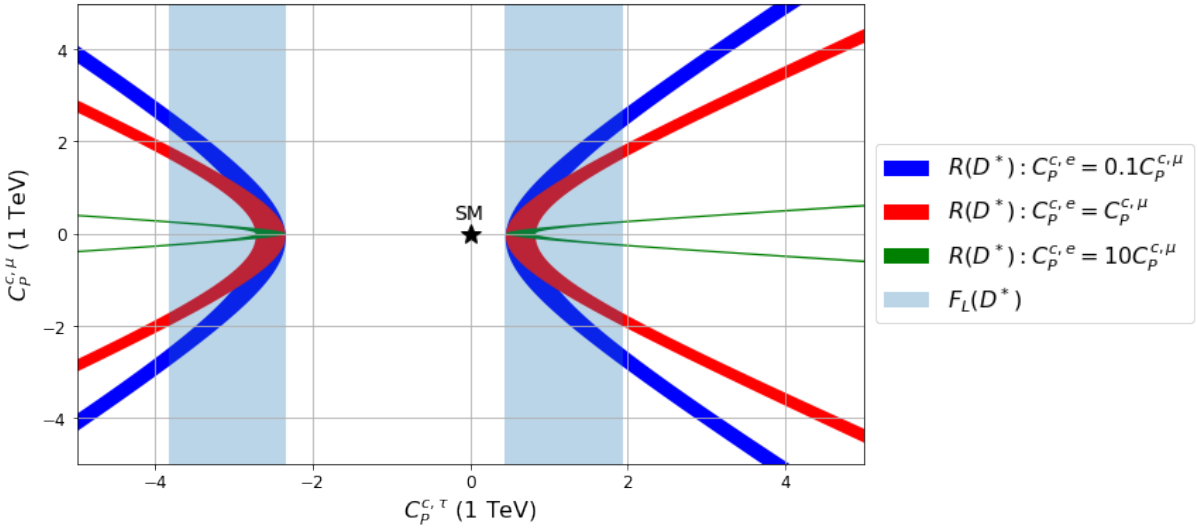

Figure 6: Bounds in the $C_P^{c,\tau}$- $C_P^{c,\mu}$ plane, for three different $C_P^{c,e}$, $C_P^{c,\mu}$ relations, derived from the observables $\mathcal{R}(\mathcal{D}^*)$ and $F_L(D^*)$. The black star corresponds to the SM values, where $C_P^{c,\tau} = C_P^{c,\mu} = 0$

Based on the overlap of the $R(D^*)$ and $F_L(D^*)$ regions in fig. 6, constraints on $C_P^{c,\mu}$ can be extrapolated. The results are presented in the second column of table 1. To potentially improve the currently determined constraints, the observable $R_\mu^e(D^*)$ is used.

$$R_\mu^e(D^*)/R_\mu^{e\,SM}(D^*) = \frac{\tilde{G}_e^{D^*}}{\tilde{G}_\mu^{D^*}} \tag{3.14}$$

Where the e and μ contribution are given by:

$$\tilde{G}_e^{D^*} = 1 + 8.981 \times 10^{-5} Re[C_P^{c,e*}] + 0.051 |C_P^{c,e}|^2 \tag{3.15}$$

$$\tilde{G}_\mu^{D^*} = 1 + 0.018 Re[C_P^{c,\mu*}] + 0.051 |C_P^{c,\mu}|^2 \tag{3.16}$$

Figure 7 plots eq. (3.14) for the three different $C_P^{c,e}$ - $C_P^{c,\mu}$ scenarios. The limits imposed by the experimental result, lead to a new constraint of $C_P^{c,\mu}$ presented in the third column of table 1. Through the relation between $C_P^{c,\tau}$ and $C_P^{c,\mu}$ as a result of $R(D^*)$, the constraints of $C_P^{c,\tau}$ can also be improved, and are presented in the last column of table 1. It can be noted that the SM value ($C_P^{c,\ell} = 0$) is not present in the presented interval for $C_P^{c,\tau}$, but is for $C_P^{c,\mu}$ and $C_P^{c,e}$.

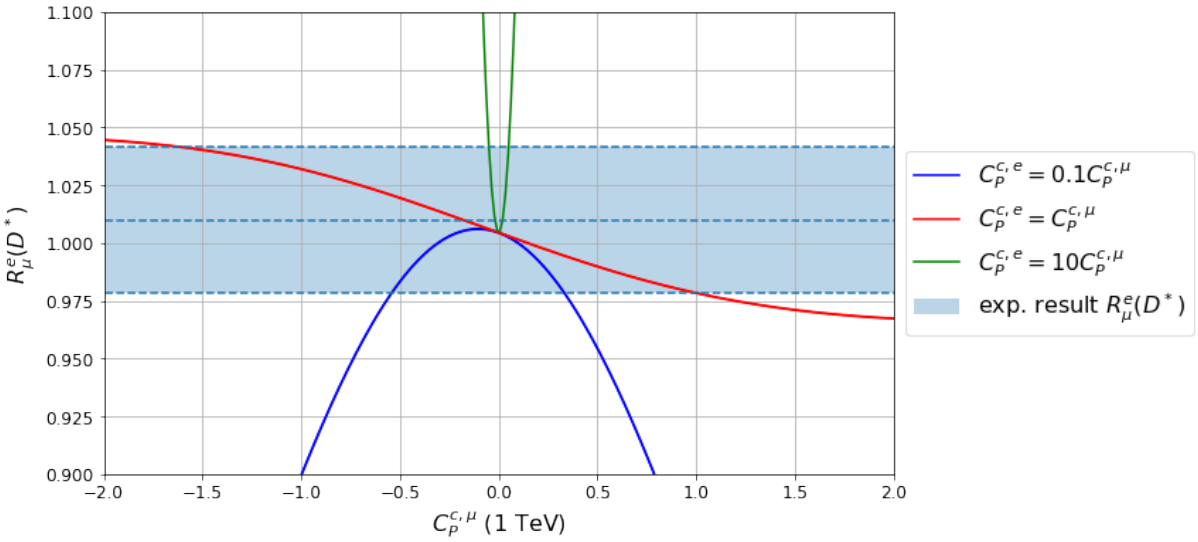

Figure 7: The observable's $R_\mu^e(D^*)$ relation to $C_P^{c,\mu}$ for three different relations with $C_P^{c,e}$. The experimental measurement of $R_\mu^e(D^*)$ allows bounds to be placed on the NP Wilson coefficient $C_P^{c,\mu}$.

Limits	$C_P^{c,\mu}$ (1 TeV)		$C_P^{c,\tau}$ (1 TeV)	
Limit parameters	$\mathcal{R}(D^*)$, $F_L(D^*)$	$R_\mu^e(D^*)$	$\mathcal{R}(D^*)$, $F_L(D^*)$	$\mathcal{R}(D^*)$, $F_L(D^*)$, $R_\mu^e(D^*)$
$C_P^{c,e} = 10C_P^{c,\mu}$	[-0.27, 0.27]	[-0.049, 0.051]	[-3.83, -2.34], [0.44, 1.94]	[-2.80, -2.34], [0.44, 0.90]
$C_P^{c,e} = C_P^{c,\mu}$	[-2.01, 1.91]	[-1.62, 1.00]	[-3.83, -2.34], [0.44, 1.94]	[-3.72, -2.34], [0.44, 1.34]
$C_P^{c,e} = 0.1C_P^{c,\mu}$	[-2.89, 2.68]	[-0.54, 0.33]	[-3.83, -2.34], [0.44, 1.94]	[-2.77, -2.34], [0.44, 0.88]

Table 1: Constraints on the NP Wilson coefficients $C_P^{c,\mu}$ and $C_P^{c,\tau}$ for three different $C_P^{c,e}$, $C_P^{c,\mu}$ relations. The observables used to compute the bounds are given in the second row.

To find these constraints, the same method as presented in Fleischer *et al.* [1] was used. Hence, we can compare our results to theirs. For each interaction type, equivalent relations were found in the $C_P^{c,\tau}$- $C_P^{c,\mu}$ plane. Small differences can be found in the numerical intervals for the pseudoscalar coefficients. It is probable these differences can largely be attributed to rounding differences of the numerical values in the equations of the observables. The deviation is largest for the $C_P^{c,e} = C_P^{c,\mu}$ scenario. This can be explained by the fact that a small deviation in $R_\mu^e(D^*)$, leads to a larger shift in $C_P^{c,\mu}$ compared to the other scenarios (see fig. 7). In this thesis, the values presented in ref. [1] were used, where instead they could have used more precise values in their computations.

3.2 Constraints on Scalar Wilson Coefficients

Like the pseudoscalar coefficients, the dependence of the observables on the scalar Wilson coefficients can be derived:

$$\mathcal{R}(D^*)/\mathcal{R}(D^*)^{SM}|_\tau = 1.00 \tag{3.17}$$

$$\mathcal{R}(D)/\mathcal{R}(D)^{SM}|_\tau = 1.00 + 1.46Re[C_S^{c,\tau *}] + 0.98|C_S^{c,\tau}|^2 \tag{3.18}$$

$$F_L(D^*) = \left(\mathcal{R}(D^*)^{SM}/\mathcal{R}(D^*)|_\tau\right)\,(0.46) \tag{3.19}$$

$\mathcal{R}(D^*)$ and $F_L(D^*)$ yield no relation to $C_S^{c,\tau}$ and hence any deviation between experimental measurements of $\mathcal{R}(D^*)$ and $F_L(D^*)$ and the SM cannot be explained by scalar NP effects. For the light generations, the following expressions are found:

$$\mathcal{R}(D^*)/\mathcal{R}(D^*)^{SM}|_{e,\mu} = \frac{1}{G_\mu^{D^*} + G_e^{D^*}} = 1 \tag{3.20}$$

$$\mathcal{R}(D)/\mathcal{R}(D)^{SM}|_{e,\mu} = \frac{1}{G_\mu^{D} + G_e^{D}} \tag{3.21}$$

With

$$G_\mu^D = 0.50 + 0.07Re[C_S^{c,\mu *}] + 0.52|C_S^{c,\mu}|^2 \tag{3.22}$$

$$G_e^D = 0.50 + 3.6 \times 10^{-4} Re[C_S^{c,e *}] + 0.53|C_S^{c,e}|^2 \tag{3.23}$$

Again, no dependence on the scalar coefficients is found for $R(D^*)$. Using eq. (3.1) a relation between $C_S^{c,\tau}$ and $C_S^{c,\mu}$ can be found by multiplying the heavy (eq. (3.18)) and light (eq. (3.21)) generations contribution. The result is plotted in fig. 8. Also $R_\mu^e(D^*)$ provides no dependence on $C_S^{c,\mu}$ and $C_S^{c,e}$. From this figure, it can be concluded that no strict constraints can be placed on the scalar Wilson coefficients. Considering the decay $B_c \to \tau\nu_\tau$ will not improve this, since its branching fraction has no dependence on the NP scalar Wilson coefficients. More experimental data from other (semi-)leptonic decay modes sensitive to NP scalar effects would be needed to provide better constraints. The SM values do not overlap with the allowed regions on the coefficients within 1σ.

The dependence of the observables on the scalar NP coefficients found and displayed in this section are consistent with the results presented in Fleischer *et al.* [1].

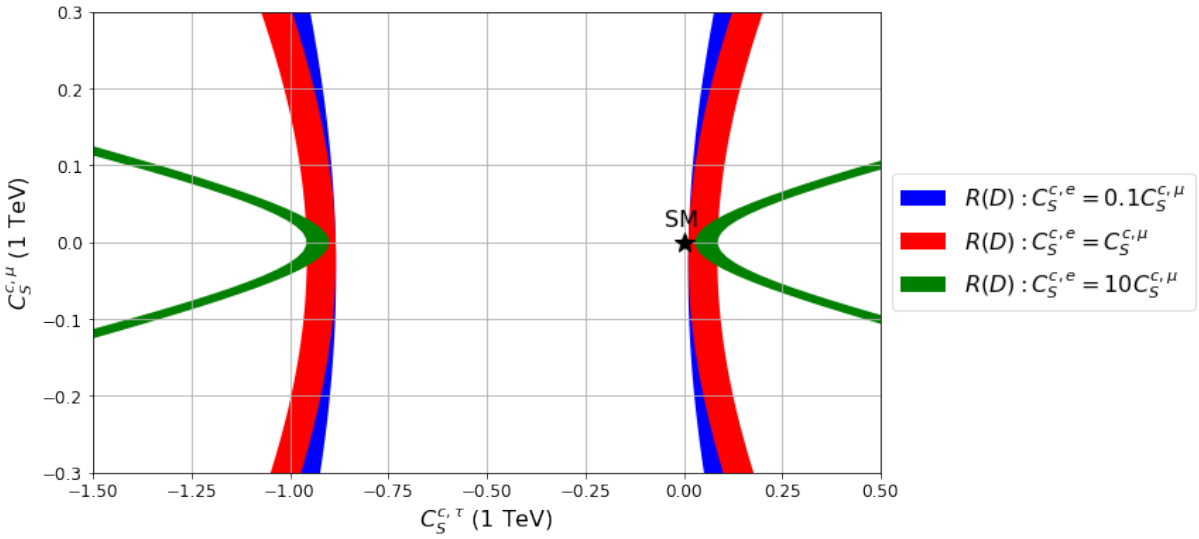

Figure 8: Constraints in the $C_S^{c,\tau}$- $C_S^{c,\mu}$ plane, for three different $C_S^{c,e}$, $C_S^{c,\mu}$ relations, derived from the observable $\mathcal{R}(\mathcal{D})$. The black star corresponds to the SM values, where $C_S^{c,\tau} = C_S^{c,\mu} = 0$

3.3 Constraints on Vector Wilson Coefficients

The left- and right-handed Wilson coefficients will be evaluated separately. At the lowest order in the SMEFT, the right-handed vector coefficient adheres to LFU, i.e. $C_{V_R}^{q,\ell} = C_{V_R}^{q}$ [1]. The observables have the following dependency on $C_{V_R}^{c}$:

$$\mathcal{R}(D^*)/\mathcal{R}(D^*)^{SM} = \frac{1 + |C_{V_R}^c|^2 - 1.80 Re(C_{V_R}^{c*})}{1 + |C_{V_R}^c|^2 - 1.752 Re(C_{V_R}^{c*})} \tag{3.24}$$

$$\mathcal{R}(D)/\mathcal{R}(D)^{SM} = 1 \tag{3.25}$$

$$F_L(D^*) = \frac{0.46|1 - C_{V_R}^c|^2}{1 + |C_{V_R}^c|^2 - 1.80 Re(C_{V_R}^{c*})} \tag{3.26}$$

$$R_\mu^e(D^*)/R_\mu^{e\,SM}(D^*) = 1 \tag{3.27}$$

Figures 9 and 10 show that the discussed observables that are related to C_{V_R} ($\mathcal{R}(D^*)$ and $F_L(D^*)$) are in disagreement with the experimental measurements. Hence, the experimental results cannot be explained by solely NP right-handed vector interactions. This is also consistent with the results found by Fleischer *et al.*

Therefore, only the left-handed coefficient will be further considered in this section. The NP effects entering through τ for the C_{V_L} NP contribution is given by:

$$\mathcal{R}(D^*)/\mathcal{R}(D^*)^{SM}|_\tau = |1 + C_{V_L}^{c,\tau}|^2 \tag{3.28}$$

$$\mathcal{R}(D)/\mathcal{R}(D)^{SM}|_\tau = |1 + C_{V_L}^{c,\tau}|^2 \tag{3.29}$$

$$F_L(D^*) = \left(\mathcal{R}(D^*)^{SM}/\mathcal{R}(D^*)|_\tau\right)\left(0.46|1 + C_{V_L}^{c,\tau}|^2\right) \tag{3.30}$$

At first glance it seems like all the expressions above are dependent on $C_{V_L}^{c,\tau}$, however, the dependence on $C_{V_L}^{c,\tau}$ for the numerator and denominator of $F_L(D^*)$ are equal and therefore cancel.

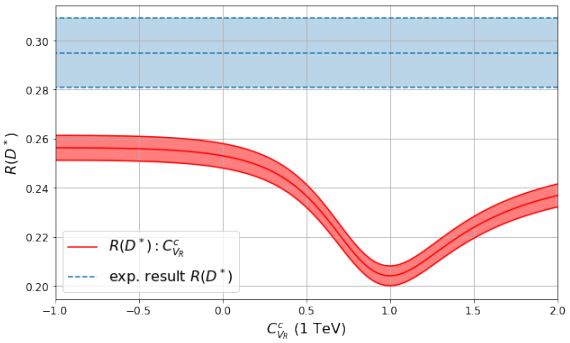

Figure 9: The observable's $\mathcal{R}(D^*)$ relation to $C^c_{V_R}$. The experimental measurement of $\mathcal{R}(D^*)$ does not overlap with the found dependency on $C^c_{V_R}$ at 1σ, hence no bounds can be placed.

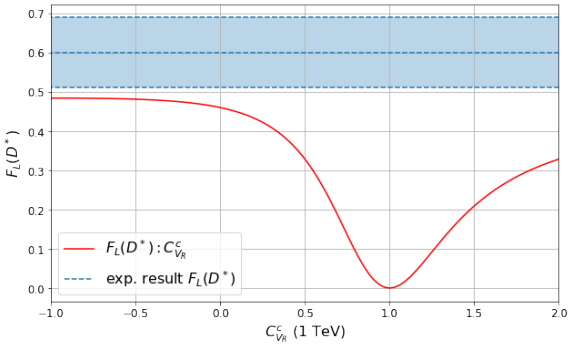

Figure 10: The observable's $F_L(D^*)$ relation to $C^c_{V_R}$. The experimental measurement of $F_L(D^*)$ does not overlap with the found dependency on $C^c_{V_R}$ at 1σ, hence no bounds can be placed.

The effects of the light generations are given by:

$$\mathcal{R}(D^*)/\mathcal{R}(D^*)^{SM}|_{e,\mu} = \frac{1}{G^{D^*}_\mu + G^{D^*}_e} \tag{3.31}$$

With

$$G^{D*}_\mu = 0.499|1 + C^{c,\mu}_{V_L}|^2, \qquad G^{D*}_e = 0.501|1 + C^{c,e}_{V_L}|^2 \tag{3.32}$$

$$\mathcal{R}(D)/\mathcal{R}(D)^{SM}|_{e,\mu} = \frac{1}{G^{D}_\mu + G^{D}_e} \tag{3.33}$$

With

$$G^{D}_\mu = 0.50|1 + C^{c,\mu}_{V_L}|^2, \qquad G^{D}_e = 0.50|1 + C^{c,e}_{V_L}|^2 \tag{3.34}$$

Based on the observables $\mathcal{R}(D)$ and $\mathcal{R}(D^*)$, the allowed regions in the $C^{c,\tau}_{V_L}$- $C^{c,\mu}_{V_L}$ plane can be plotted (fig. 11). However, these regions are not bounded and therefore do not yield strict constraints. Figure 12 shows the regions around the SM value, showing that it falls outside the 1σ constraints.

The observable $R^e_\mu(D^*)$ is related to $C^{c,\mu}_{V_L}$ and $C^{c,e}_{V_L}$, and is given by:

$$R^e_\mu(D^*)/R^{e\ SM}_\mu(D^*) = \frac{\tilde{G}^{D^*}_e}{\tilde{G}^{D^*}_\mu} \tag{3.35}$$

Where the e and μ contribution are given by:

$$\tilde{G}^{D^*}_e = |1 + C^{c,e}_{V_L}|^2, \qquad \tilde{G}^{D^*}_\mu = |1 + C^{c,\mu}_{V_L}|^2 \tag{3.36}$$

Figure 13 shows that $R^e_\mu(D^*)$ does lead to bounds on $C^{c,\mu}_{V_L}$ and $C^{c,e}_{V_L}$. Except for when $C^{c,\mu}_{V_L} = C^{c,e}_{V_L}$. The resulting constraints are presented in the second column of table 2. Based on the relation between $C^{c,\tau}_{V_L}$ and $C^{c,\mu}_{V_L}$ as shown in fig. 11, constraints on $C^{c,\tau}_{V_L}$ can be extrapolated and are presented in the third column of table 2.

Similar to the pseudoscalar, the found constraints can be compared to Fleischer *et al.* [1]. Again for each interaction type, equivalent relations were found in the $C^{c,\tau}_{V_R}$- $C^{c,\mu}_{V_R}$ plane. The small deviations that are present can still be ascribed to rounding differences of the values in the used expressions.

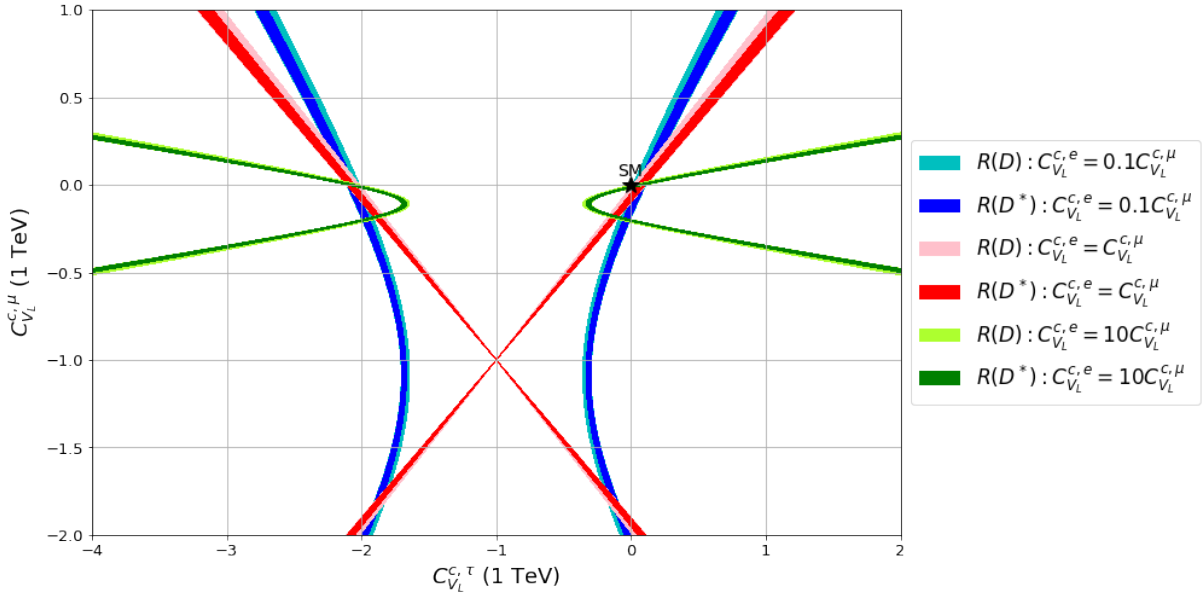

Figure 11: Constraints in the $C_{V_L}^{c,\tau}$- $C_{V_L}^{c,\mu}$ plane, for three different $C_{V_L}^{c,e}$, $C_{V_L}^{c,\mu}$ relations, derived from the observables $\mathcal{R}(\mathcal{D})$ and $\mathcal{R}(\mathcal{D}^*)$. The black star corresponds to the SM values, where $C_{V_L}^{c,\tau} = C_{V_L}^{c,\mu} = 0$.

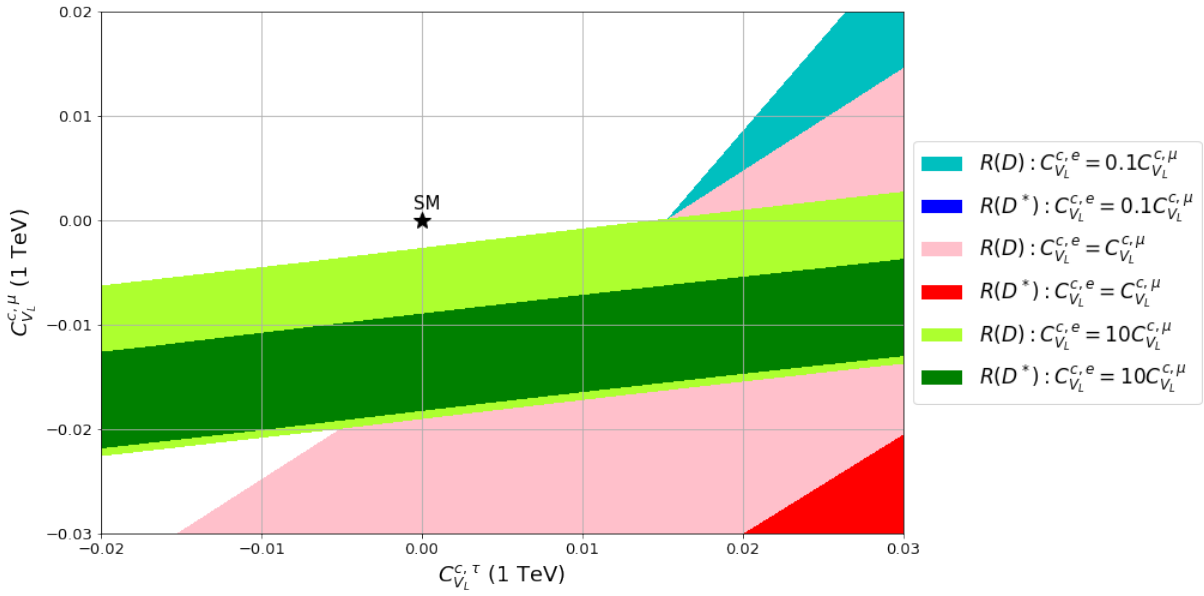

Figure 12: The same relations as shown in fig. 11, zoomed in on the region around the SM value.

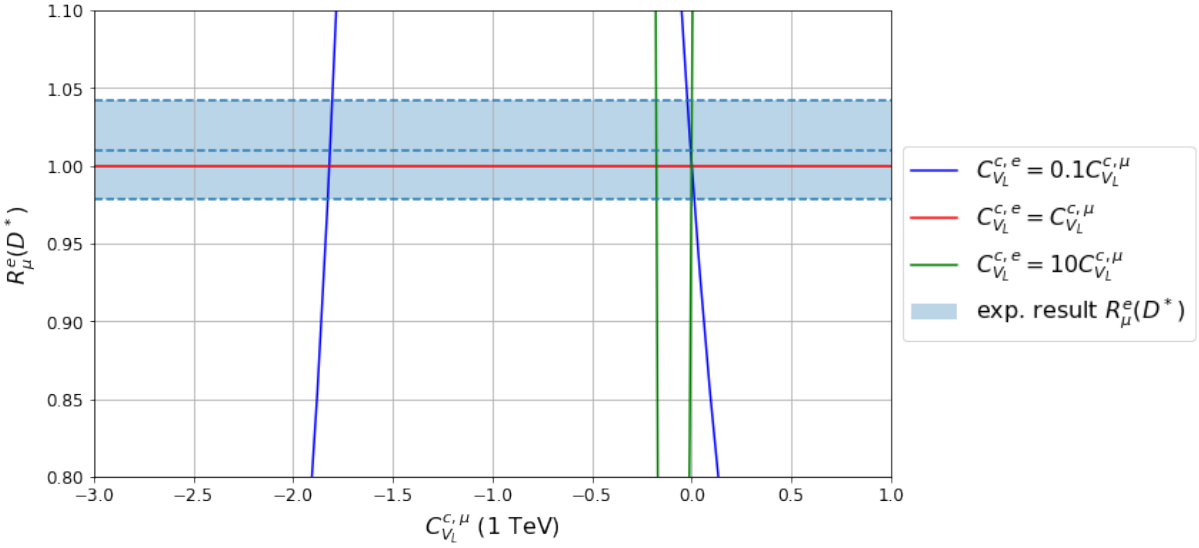

Figure 13: The observable's $R_\mu^e(D^*)$ relation to $C_{V_L}^{c,\mu}$ for three different relations with $C_{V_L}^{c,e}$. The experimental measurement of $R_\mu^e(D^*)$ allows bounds to be placed on the NP Wilson coefficient $C_{V_L}^{c,\mu}$.

Limits	$C_{V_L}^{c,\mu}$ (1 TeV)	$C_{V_L}^{c,\tau}$ (1 TeV)
Limit parameters	$R_\mu^e(D^*)$	$\mathcal{R}(D^*)$, $\mathcal{R}(D)$ and $R_\mu^e(D^*)$
$C_{V_L}^{c,e} = 10C_{V_L}^{c,\mu}$	[-0.183, -0.181] [-0.0012, 0.0023]	[-1.917, -1.827] ∪ [-0.173, -0.083] [-2.126, -2.009] ∪ [0.0086, 0.126]
$C_{V_L}^{c,e} = 0.1C_{V_L}^{c,\mu}$	[-1.826,-1.803] [-0.0224, 0.0122]	[-1.913, -1.824] ∪ [-0.176, -0.086] [-2.111, -2.003] ∪ [0.0028, 0.119]

Table 2: Constraints on the NP Wilson coefficients $C_{V_L}^{c,\mu}$ and $C_{V_L}^{c,\tau}$ for two different $C_{V_L}^{c,e}$, $C_{V_L}^{c,\mu}$ relations. The observables used to compute the bounds are given in the second row.

3.4 Constraints on Tensor Wilson Coefficients

The final situation that is evaluated is NP entering through the tensor Wilson coefficients. The effects from τ are given by the following equations:

$$\mathcal{R}(D^*)/\mathcal{R}(D^*)^{SM}|_\tau = 1 - 5.02Re[C_T^{c,\tau *}] + 15.94|C_T^{c,\tau}|^2 \tag{3.37}$$
$$\mathcal{R}(D)/\mathcal{R}(D)^{SM}|_\tau = 1 + 1.14Re[C_T^{c,\tau *}] + 0.91|C_T^{c,\tau}|^2 \tag{3.38}$$
$$F_L(D^*) = \left(\mathcal{R}(D^*)^{SM}/\mathcal{R}(D^*)|_\tau\right)\left(0.46 - 1.95Re(C_T^{c,\tau *}) + 3.08|C_T^{c,\tau}|^2\right) \tag{3.39}$$

It is found that the expression for $F_L(D^*)$ does not intersect with the experimental data. Hence, at the 1σ level, it can already be concluded that C_T cannot be the only NP contribution based on the observables that are currently analysed. Despite this, the possible regions in the $C_T^{c,\tau}$-$C_T^{c,\mu}$ plane can still be examined. Therefore, the effect of e, μ on $\mathcal{R}(\mathcal{D}^*)$ and $\mathcal{R}(\mathcal{D})$ are needed:

$$\mathcal{R}(D^*)/\mathcal{R}(D^*)^{SM}|_{e,\mu} = \frac{1}{G_\mu^{D^*} + G_e^{D^*}} \tag{3.40}$$

With

$$G_\mu^{D*} = 0.499 - 0.221Re[C_T^{c,\mu *}] + 7.710|C_T^{c,\mu}|^2 \tag{3.41}$$
$$G_e^{D*} = 0.501 - 0.001Re[C_T^{c,e *}] + 7.743|C_T^{c,e}|^2 \tag{3.42}$$

$$\mathcal{R}(D)/\mathcal{R}(D)^{SM}|_{e,\mu} = \frac{1}{G_\mu^{D} + G_e^{D}} \tag{3.43}$$

With

$$G_\mu^{D} = 0.50 + 0.10Re[C_T^{c,\mu *}] + 0.37|C_T^{c,\mu}|^2 \tag{3.44}$$
$$G_e^{D} = 0.50 + 5.0 \times 10^{-4}Re[C_T^{c,e *}] + 0.37|C_T^{c,e}|^2 \tag{3.45}$$

The resulting regions are shown in fig. 14. With fig. 15 showing the area around the SM value, from which can be seen it is in disagreement with the found regions.

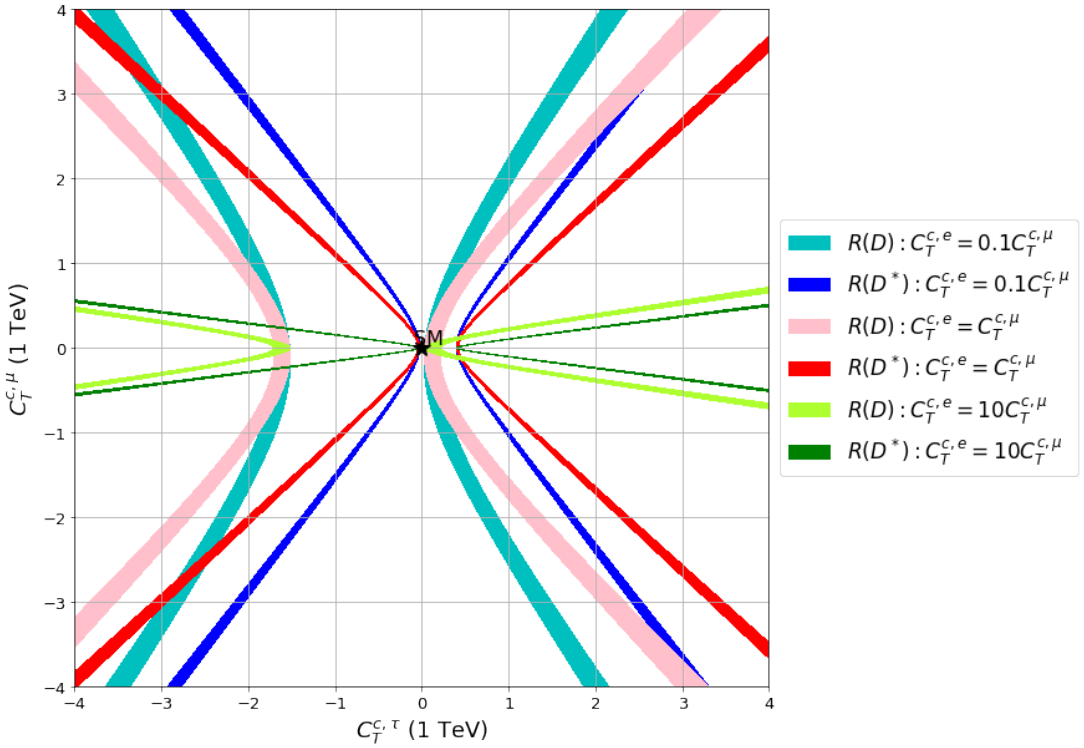

Figure 14: Constraints in the $C_T^{c,\tau}$- $C_T^{c,\mu}$, for three different $C_T^{c,e}$, $C_T^{c,\mu}$ relations, derived from the observables $\mathcal{R}(\mathcal{D})$ and $\mathcal{R}(\mathcal{D}^*)$. The black star corresponds to the SM values.

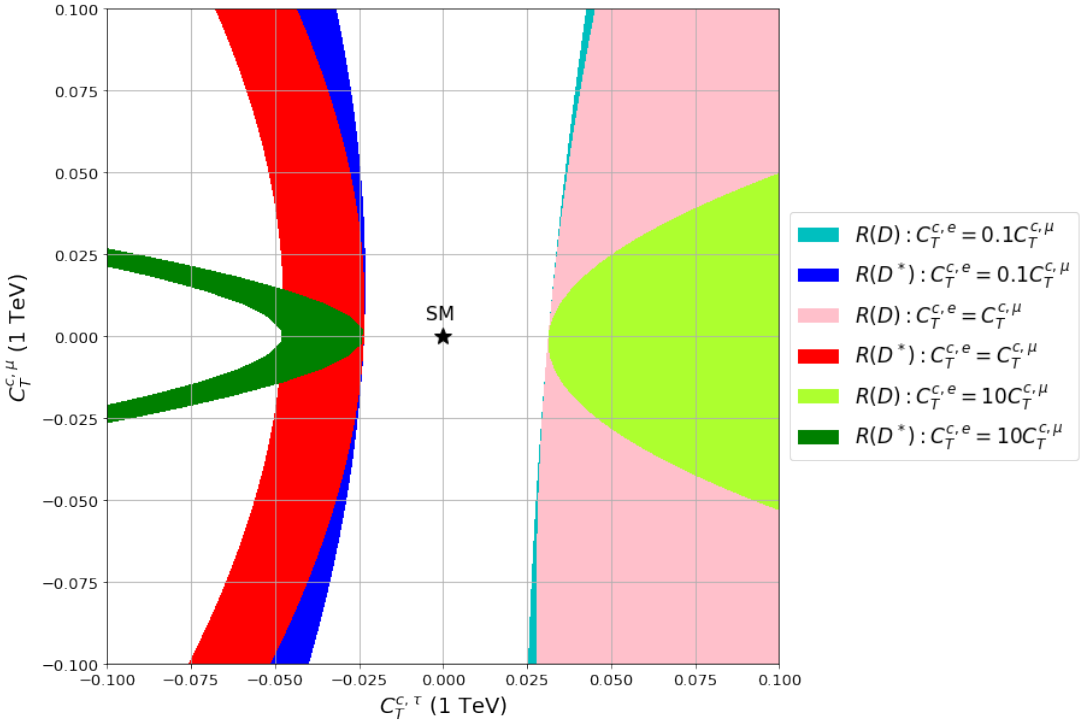

Figure 15: The same relations as shown in fig. 14, zoomed in on the region around the SM value.

Additionally, the relation to the observable $R_\mu^e(D^*)$ and the resulting bounds on $C_T^{c,e}$ and $C_T^{c,\mu}$ can be analysed:

$$R_\mu^e(D^*)/R_\mu^{e\,SM}(D^*) = \frac{\tilde{G}_e^{D^*}}{\tilde{G}_\mu^{D^*}} \tag{3.46}$$

With

$$\tilde{G}_e^{D^*} = 1 + 2.164 \times 10^{-3} Re[C_T^{c,e*}] + 15.455|C_T^{c,e}|^2 \tag{3.47}$$

$$\tilde{G}_\mu^{D^*} = 1 + 0.433 Re[C_T^{c,\mu*}] + 15.458|C_T^{c,e}|^2 \tag{3.48}$$

$R_\mu^e(D^*)$ does result in constraints on $C_T^{c,\mu}$ (see fig. 16), the corresponding numerical values of the allowed intervals of $C_T^{c,\mu}$ at the 1σ level can be found in table 3.

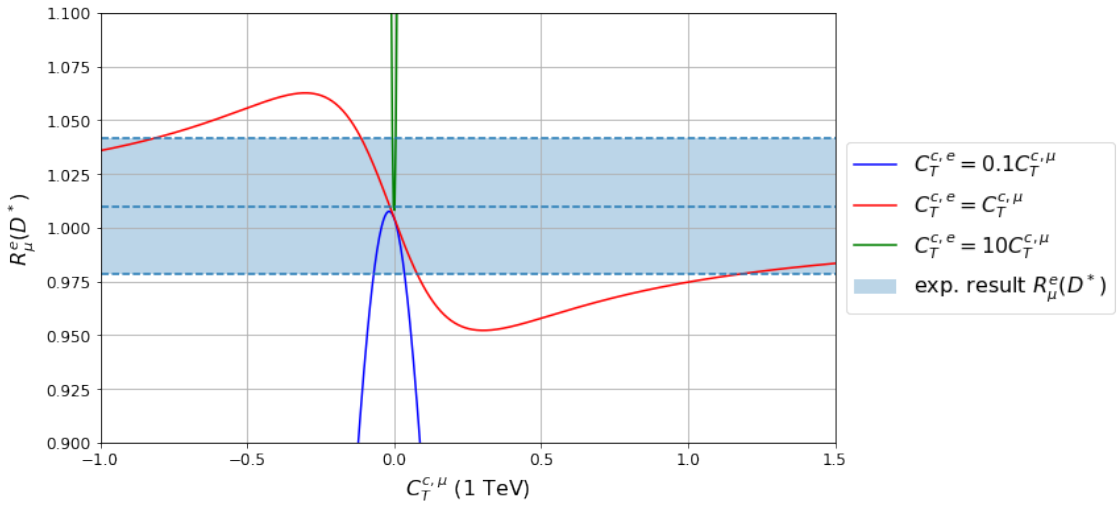

Figure 16: The observable's $R_\mu^e(D^*)$ relation to $C_T^{c,\mu}$ for three different relations with $C_T^{c,\mu}$. The experimental measurement of $R_\mu^e(D^*)$ allows bounds to be placed on the NP Wilson coefficient $C_{V_T}^{c,\mu}$.

Limits	$C_T^{c,\mu}$ (1 TeV)
Limit parameters	$R_\mu^e(D^*)$
$C_T^{c,e} = 10C_T^{c,\mu}$	[-0.0060, 0.0064]
$C_T^{c,e} = 1C_T^{c,\mu}$	(-∞, 0.695], [-0.131, 0.064], [1.45,∞)
$C_T^{c,e} = 0.1C_T^{c,\mu}$	[-0.065, 0.031]

Table 3: Constraints on the NP Wilson coefficient $C_{V_L}^{c,\mu}$ for three different $C_{V_L}^{c,e}$, $C_{V_L}^{c,\mu}$ relations, based on the experimental measurements of $R_\mu^e(D^*)$.

The relation shown in fig. 16 is not in full agreement with Fleischer *et al.* It appears the sign of $C_T^{c,\mu}$ has to be reversed to obtain the same relations. Upon close examination of the expression of $R_\mu^e(D^*)$ provided by Fleischer *et al.* and eqs. (3.46) to (3.48), which are derived from the expression by the paper, no inconsistencies are found, which could indicate an error by Fleischer *et al.* The constraints derived from $\mathcal{R}(\mathcal{D})$ and $\mathcal{R}(\mathcal{D}^*)$ (fig. 14) are consistent with Fleischer *et al.*

4 Potential impact of a $B_c \to \tau\nu_\tau$ measurement

In combination with the constraints determined in section 3, the potential impact of a measurement of the $B_c \to \tau\nu_\tau$ decay on the NP coefficients will be analysed. At the energy scale $\mu = m_b$, the ratio between the branching fraction of the B_c decay and its SM prediction is defined by the following equation: [1]

$$\mathcal{B}(B_c \to \tau\nu_\tau)/\mathcal{B}(B_c \to \tau\nu_\tau)^{\text{SM}} = |1 + C_{V_L}^{c,\tau} + 4.06 C_P^{c,\tau}|^2 \tag{4.1}$$

Where

$$\mathcal{B}(B_c \to \tau\nu_\tau)^{\text{SM}} = \frac{G_F^2}{8\pi}|V_{cb}|^2 M_{B_c} m_\tau^2 \left(1 - \frac{m_\tau^2}{M_{B_c}^2}\right)^2 f_{B_c}^2 \tau_{B_c} \tag{4.2}$$

Where G_F is the Fermi coupling constant, M_{B_c} is the mass of B_c, m_τ is the mass of the τ lepton, f_{B_c} is the B_c meson decay constant and τ_{B_c} is the lifetime of B_c. Unlike the previously discussed ratios in section 3, the ratio in eq. (4.1) is not independent of the CKM element $|V_{cb}|$. To compute this ratio, inclusive and exclusively determined value of $|V_{cb}|$ are used. Their values were presented in section 2.1.1 [9].

To compute the branching fraction, natural units are used ($\hbar = c = 1$). Additionally, the units of the B_c lifetime need to be converted from seconds to GeV^{-1} using the conversion factor: $1\text{s} = 6.582 \times 10^{-25}\ \text{GeV}^{-1}$. The result of the eq. (4.2) for the external $|V_{cb}|$ value is:

$$\mathcal{B}(B_c \to \tau\nu_\tau)^{\text{SM}}_{\text{excl.}} = (2.07 \pm 0.20) \times 10^{-2} \tag{4.3}$$

Which is not in full agreement with [1], which states the following value for the branching fraction:

$$\mathcal{B}(B_c \to \tau\nu_\tau)^{\text{SM}}_{\text{excl.}} = (2.25 \pm 0.21) \times 10^{-2} \tag{4.4}$$

For the inclusive determination of $|V_{cb}|$ the corresponding SM branching fraction is:

$$\mathcal{B}(B_c \to \tau\nu_\tau)^{\text{SM}}_{\text{incl.}} = (2.29 \pm 0.19) \times 10^{-2} \tag{4.5}$$

Equation (4.1) shows that the branching fraction of $B_c \to \tau\nu_\tau$ is dependent on the pseudoscalar and left-handed vector Wilson coefficient. On the other hand, this implies it cannot be used to put constraints on the NP scalar, tensor and right-handed vector Wilson coefficients. An experimental measurement of the branching fraction could help constrain $C_P^{c,\ell}$ and $C_{V_L}^{c,\ell}$ further. Ref. [1, 27] argue that bounds on the branching fraction stricter than 60% cannot be placed, considering the limits on the NP parameter space and the contributions of the $B_c \to \tau\nu_\tau$ decay. Hence, in this analysis 60% will be taken as an upper bound, but the effect of lower values will still be examined.

$$\mathcal{B}(B_c \to \tau\nu_\tau) < 0.60 \tag{4.6}$$

4.1 Impact on the Pseudo-scalar Wilson Coefficients

Figure 17 shows the relation between $C_P^{c,\tau}$, $|V_{cb}|$ and the branching fraction. The bounds used for $C_P^{c,\tau}$ come from table 1. For each scenario, the new constraint from $B_c \to \tau\nu_\tau$ resolves the 2-fold ambiguity by eliminating the negative interval of $C_P^{c,\tau}$. From fig. 17 it can be concluded that values $\mathcal{B}(B_c \to \tau\nu_\tau) < 0.356$ are in disagreement with experimental results at 1σ if NP effects come exclusively from pseudoscalar interactions. Or in other words, the branching fraction would have to be more than 17 times greater than its SM prediction to be consistent with the NP

scenario derived from $\mathcal{R}(D^*)$, $F_L(D^*)$ and $R^e_\mu(D^*)$. Furthermore, for all relations between $C_P^{c,e}$ and $C_P^{c,\mu}$, an upper bound of 0.614 is found for $C_P^{c,\tau}$ at 1σ, using the exclusive $|V_{cb}|$ value. Using the regions in $C_P^{c,\tau}$ - $C_P^{c,\mu}$ (fig. 6) that were established using $\mathcal{R}(\mathcal{D}^*)$ and $F_L(D^*)$, new constraints for $C_P^{c,e}$ and $C_P^{c,\mu}$ can be found. Compared to the bounds that were given in table 1, only the constraints of the $C_P^{c,e} = C_P^{c,\mu}$ scenario are improved. Table 4 shows the updated constraints. Note that for $C_P^{c,\mu}$ and $C_P^{c,e}$, the SM value is still within the given intervals.

The same analysis can be performed for the inclusive $|V_{cb}|$ value, for which similar results are found. In this case the upper bound of $C_P^{c,\tau}$ is found to be 0.607. Concerning the branching fraction, values $\mathcal{B}(B_c \to \tau\nu_\tau) < 0.363$ are in disagreement with experimental results at 1σ if NP effects come exclusively from pseudoscalar interactions. The final updated constraints for $C_P^{c,\tau}$ and $C_P^{c,\mu}$ are presented in table 4.

Limits	$C_P^{c,\mu}$ (1 TeV)		$C_P^{c,\tau}$ (1 TeV)	
V_{cb}	excl.	incl.	excl.	incl.
$C_P^{c,e} = 10C_P^{c,\mu}$	[-0.049, 0.051]	[-0.049, 0.051]	[0.44, 0.61]	[0.44, 0.61]
$C_P^{c,e} = C_P^{c,\mu}$	[-0.59, 0.48]	[-0.58, 0.47]	[0.44, 0.61]	[0.44, 0.61]
$C_P^{c,e} = 0.1C_P^{c,\mu}$	[-0.54, 0.33]	[-0.54, 0.33]	[0.44, 0.61]	[0.44, 0.61]

Table 4: Constraints on the NP Wilson coefficients $C_P^{c,\mu}$ and $C_P^{c,\tau}$ for three different $C_P^{c,e}$ - $C_P^{c,\mu}$ relations and the inclusive and exclusive determination of $|V_{cb}|$. $\mathcal{R}(D^*)$, $F_L(D^*)$ and $R^e_\mu(D^*)$ were used to compute the bounds in combination with $\mathcal{B}(B_c \to \tau\nu_\tau) < 0.60$.

4.2 Impact on the Left-handed Vector Wilson Coefficients

For the left-handed vector coefficient, a full agreement between the previously determined bounds for the coefficient and $|V_{cb}|$ can be found together with the 60% limit of the branching fraction, as can be seen in fig. 18. The contour lines of the branching fraction show that the overlapping regions correspond to a branching fraction similar to the SM prediction. The numerical values of the branching fraction limits at the 1σ level are given in table 5.

For the NP left-handed vector coefficients, Fleischer *et al.* [1] claims the limit on the branching fraction at 60% eliminates two of the four regions found previously in the $C_{V_L}^{c,\tau}$- $C_{V_L}^{c,\mu}$ plane (see table 2), specifically those corresponding to branching fractions smaller than the SM estimate. This is not in agreement with the regions found in the $C_{V_L}^{c,\tau}$- $|V_{cb}|$ plane, which correspond to branching fraction values of around $\sim 0.01 - 0.03$ (see fig. 18).

Limits	$\mathcal{B}(B_c \to \tau\nu_\tau)$	
V_{cb}	excl.	incl.
$C_{V_L}^{c,e} = 10C_{V_L}^{c,\mu}$	[0.0134, 0.0185], [0.0199, 0.0279]	[0.0151, 0.0195], [0.0224, 0.0294]
$C_{V_L}^{c,e} = 0.1C_{V_L}^{c,\mu}$	[0.0133, 0.0184], [0.0196, 0.0271]	[0.0150, 0.0194], [0.0222, 0.0291]

Table 5: Constraints on the $B_c \to \tau\nu_\tau$ branching fraction, for the scenario where NP effects are coming from left-handed vector interactions only. Computed for two different $C_{V_L}^{c,e}$ - $C_{V_L}^{c,\mu}$ scenarios, together with the inclusive and exclusive determination of $|V_{cb}|$.

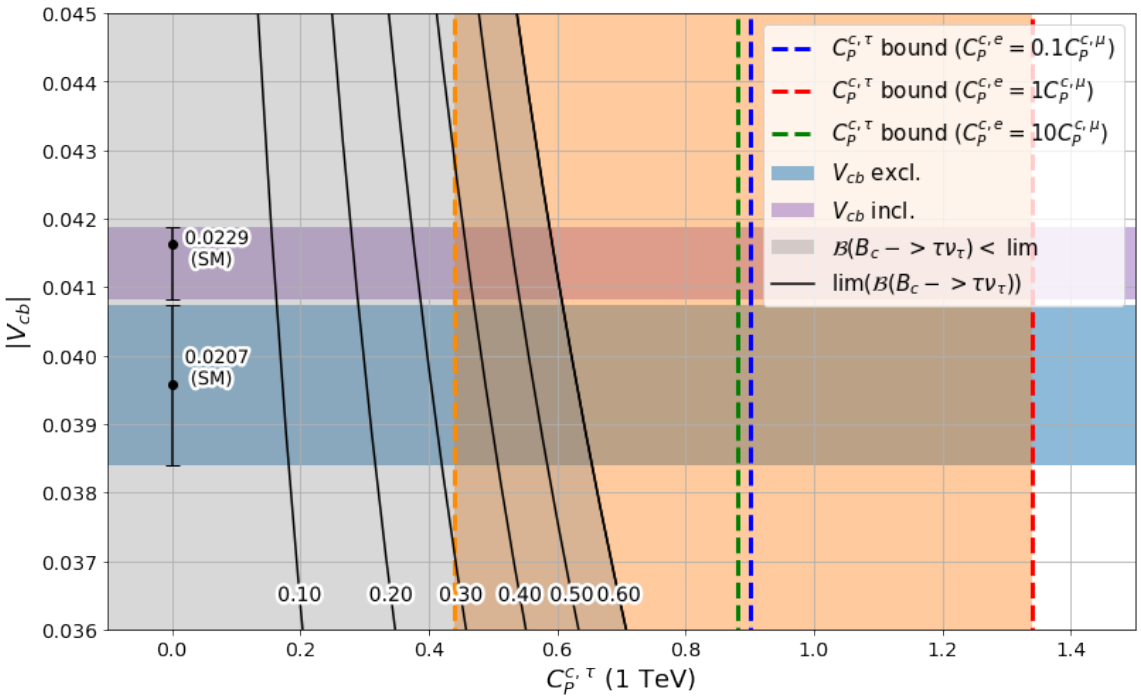

Figure 17: The relation of the branching fraction of $B_c \to \tau\nu_\tau$ to the CKM element V_{cb} and $C_P^{c,\tau}$. The $C_P^{c,\tau}$ constraints for three different $C_P^{c,e}$, $C_P^{c,\mu}$ relations are displayed together with the inclusive and exclusive determination of $|V_{cb}|$. The values in the plot are branching fractions corresponding to the contour lines or data points. The overlap between the regions allow new improved constraints to be placed on $C_P^{c,\tau}$.

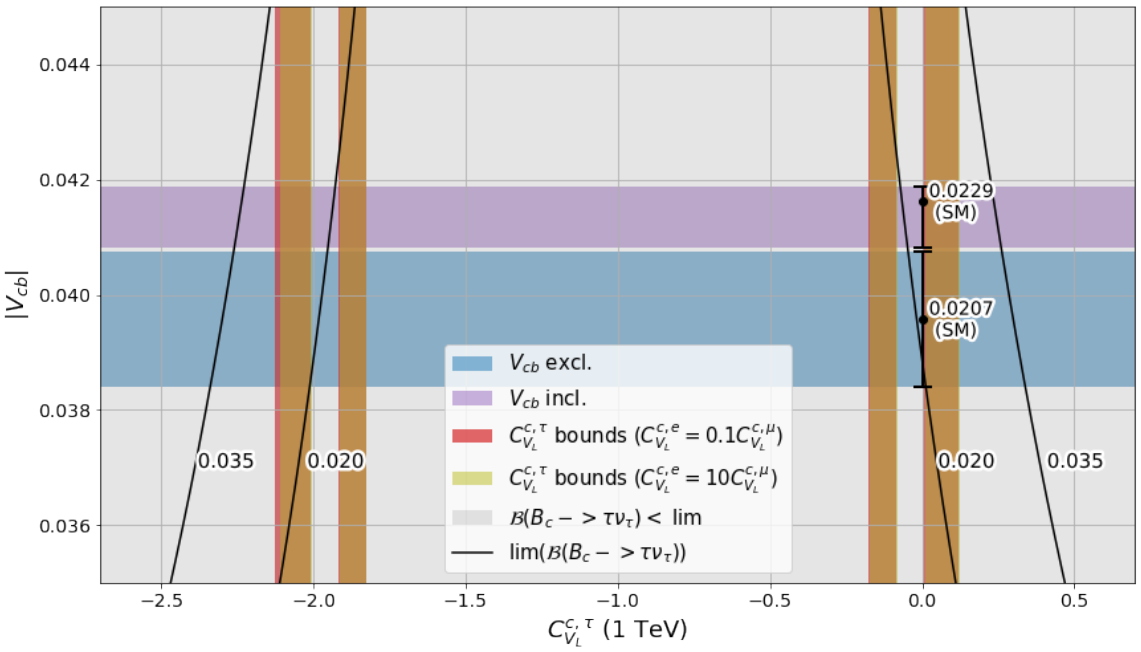

Figure 18: The relation of the branching fraction of $B_c \to \tau\nu_\tau$ to the CKM element V_{cb} and $C_{V_L}^{c,\tau}$. The $C_{V_L}^{c,\tau}$ constraints for two different $C_{V_L}^{c,e}$ - $C_{V_L}^{c,\mu}$ scenarios are displayed. The range of the branching fraction values in the overlapping regions is close to the SM estimate.

5 Conclusion

Shortcomings of the standard model have led physicists to search for physics beyond the SM or new physics. The LHCb experiment does this by comparing experimental measurements to their SM estimates. In this thesis, the methodology used to explore the NP parameters space is the operator product expansion, using effective field theory to make computations of weak interactions feasible. This is achieved by focusing on a single energy scale without having to know the underlying theory at higher energy scales.

To find constraints on NP Wilson coefficients corresponding to $b \to c\ell\bar{\nu}_\ell$ transitions, the work by Fleischer *et al.* [1] was followed. Based on different observables defined by ratios of various branching fractions and decay widths, combined with their experimental measurements, the NP coefficients were constrained. The coefficients are also dependent on lepton flavour. To simplify the analysis and keep it model-independent, three scenarios were considered: $C_a^e < C_a^\mu$, $C_a^e = C_a^\mu$ and $C_a^e > C_a^\mu$. For all constraints, there is an agreement with the SM between the (1-2)σ level. Only for the pseudoscalar and left-handed vector interactions strict constraints could be placed on the coefficients. The results found are consistent with Fleischer *et al.* The difference in the quantitative values of the intervals can be largely contributed to rounding differences.

The LHCb group is planning to measure the tauonic decay of the B_c meson. Therefore, the potential impact of such a measurement on the NP Wilson coefficients was explored in section 4. The branching fraction of $B_c \to \tau\nu_\tau$ decay is only sensitive to NP effects from pseudoscalar and left-handed vector operators. Additionally, the branching fraction is dependent on the CKM element V_{cb}, unlike the other observables used in the analysis. Consequently, the impact was analysed for both the exclusive and inclusively determined value of $|V_{cb}|$.

Assuming the $B_c \to \tau\nu_\tau$ branching fraction to be 60%, the pseudoscalar constraints of $C_P^{c,\mu}$ for the $C_P^{c,e} = C_P^{c,\mu}$ scenario could be improved. Additionally, for all scenarios, it was able to remove the 2-fold ambiguity that was present in $C_P^{c,\tau}$. If the NP effects enter through pseudoscalar interactions at the 1 TeV energy scale only and results that are consistent with the observables ($\mathcal{R}(D^*)$, $F_L(D^*)$ and $R_\mu^e(D^*)$) are taken, the branching fraction is expected to be $\sim 17-30$ times greater than the SM estimate. If the NP effects come from only left-handed vector interactions, the branching fraction is $\sim 0.5-1.5$ the value of the SM estimate. Due to the regions at the 1σ level being close to the SM estimate, no improvements could be made to the left-handed vector Wilson coefficients constraints.

In this thesis, we have shown that a measurement of $B_c \to \tau\nu_\tau$ could eliminate ambiguity and improve the precision of constraints in the NP parameters space. To provide more definitive proof of the existence of NP, a 5σ discrepancy with the SM needs to be found, which is not satisfied by the results presented in this thesis. To potentially achieve this, more precise experimental measurements of a wider range of observables are needed. The measurement of $B_c \to \tau\nu_\tau$ is a step in this direction. Additionally, measurements of semileptonic decays including light-generation leptons would be interesting. If the decay modes of electrons and muons are measured separately, it would also allow for improved limits on lepton flavour universality between the two. The picture of the NP parameter space is ever involving and more insight is gained by the day. We look forward to seeing what the future holds.

6 Acknowledgements

First and foremost, I would like to thank my supervisor Kristof for the great support during the past three months in which I did this research project. Whenever I had a question or needed some advice on how to proceed, he was there to help and was always available for feedback. Starting this project, I knew very little about this research field and Kristof helped me understand the basics and helped me to get started on the analysis. I would also like to thank everyone at the Van Swinderen Institute. I felt very welcome and had a great time during the project. Lastly, I would like to thank my friends and family for their support and encouragement. They were always there to listen to me and give me advice and feedback, even if my research was a mystery to them.

References

[1] R. Fleischer, R. Jaarsma, and G. Tetlalmatzi-Xolocotzi, "Mapping out the space for new physics with leptonic and semileptonic $B_{(c)}$ decays," *The European Physical Journal C*, vol. 81, no. 7, Jul. 2021. DOI: 10.1140/epjc/s10052-021-09419-8.

[2] CERN, *The matter-antimatter asymmetry problem | CERN*, Home.cern, 2019. [Online]. Available: https://home.cern/science/physics/matter-antimatter-asymmetry-problem.

[3] B. S. Ryden, *Introduction to cosmology*. Cambridge University Press, 2017.

[4] A. O. Sushkov, W. J. Kim, D. A. R. Dalvit, and S. K. Lamoreaux, "New Experimental Limits on Non-Newtonian Forces in the Micrometer Range," *Physical Review Letters*, vol. 107, no. 17, Oct. 2011. DOI: 10.1103/physrevlett.107.171101.

[5] B. Kortman, "Constraining the Standard Model effective field theory Wilson coefficients using Higgs and diboson data," Nov. 2019.

[6] A. Buonaura, "Tests of lepton flavour universality at LHCb," *Journal of Physics: Conference Series*, vol. 1586, p. 012 031, Aug. 2020. DOI: 10.1088/1742-6596/1586/1/012031.

[7] B. R. Martin and G. Shaw, *Nuclear and particle physics: An introduction*, 3rd ed. Wiley, 2019.

[8] M. Gell-Mann, "A schematic model of baryons and mesons," *Physics Letters*, vol. 8, no. 3, pp. 214–215, Feb. 1964. DOI: 10.1016/S0031-9163(64)92001-3.

[9] F. Maat, *An analysis of the standard model prediction for* $\mathcal{B}(B_c^+ \to \tau^+\nu_\tau)$, Nov. 2022.

[10] Z.-J. Xiao and X. Liu, *The two-body hadronic decays of* B_c *meson in the perturbative QCD approach: A short review*, Jul. 2014. arXiv: 1401.0151 [hep-ph].

[11] Belle Collaboration *et al.*, "Measurement of $\mathcal{R}(D)$ and $\mathcal{R}(D^*)$ with a Semileptonic Tagging Method," *Physical Review Letters*, vol. 124, no. 16, Apr. 2020. DOI: 10.1103/physrevlett.124.161803.

[12] Y. Amhis *et al.*, "Averages of b-hadron, c-hadron, and τ-lepton properties as of 2018," *The European Physical Journal C*, vol. 81, no. 3, Mar. 2021. DOI: 10.1140/epjc/s10052-020-8156-7.

[13] LHCb collaboration and A. Seuthe, "Lepton flavour universality tests at LHCb," May 2023. arXiv: 2305.08216 [hep-ex].

[14] G. Aad *et al.*, "Observation of a new particle in the search for the Standard Model Higgs boson with the ATLAS detector at the LHC," *Physics Letters B*, vol. 716, no. 1, pp. 1–29, Sep. 2012. DOI: 10.1016/j.physletb.2012.08.020.

[15] LHCb collaboration *et al.*, "The LHCb upgrade I," 2023. arXiv: 2305.10515 [hep-ex].

[16] A. Lopes, *New LHCb analysis still sees previous intriguing results*, CERN, Mar. 2020. [Online]. Available: https://home.cern/news/news/physics/new-lhcb-analysis-still-sees-previous-intriguing-results (visited on 06/17/2023).

[17] A. Falkowski and K. Mimouni, "Model independent constraints on four-lepton operators," *Journal of High Energy Physics*, vol. 2016, no. 2, Feb. 2016. DOI: 10.1007/jhep02(2016)086.

[18] E. Fermi, "Tentativo di una Teoria Dei Raggi β," *Il Nuovo Cimento*, vol. 11, pp. 1–19, Jan. 1934. DOI: 10.1007/bf02959820.

[19] K.A.M. de Bruyn, *OSAF Topical Lectures on Effective Field Theories: Application of EFTs for B Physics*, Apr. 2023.

[20] K.A.M. de Bruyn, "Searching for penguin footprints: Towards high precision CP violation measurements in the B meson systems," Apr. 2015.

[21] Particle Data Group and K. Olive, "Review of Particle Physics," *Chinese Physics C*, vol. 38, no. 9, p. 090 001, Aug. 2014. DOI: 10.1088/1674-1137/38/9/090001.

[22] G. Buchalla, A. J. Buras, and M. E. Lautenbacher, "Weak decays beyond leading logarithms," *Rev. Mod. Phys.*, vol. 68, pp. 1125–1144, 1996. DOI: 10.1103/RevModPhys.68.1125. arXiv: hep-ph/9512380.

[23] Y. Sakaki, R. Watanabe, M. Tanaka, and A. Tayduganov, "Testing leptoquark models in $\bar{B} \to D^{(*)}\tau\bar{\nu}$," *Physical Review D*, vol. 88, no. 9, Nov. 2013. DOI: 10.1103/physrevd.88.094012.

[24] S. Iguro, M. Takeuchi, and R. Watanabe, "Testing leptoquark/EFT in $\bar{B} \to D^{(*)}\ell\bar{\nu}$ at the LHC," *The European Physical Journal C*, vol. 81, no. 5, May 2021. DOI: 10.1140/epjc/s10052-021-09125-5.

[25] Belle Collaboration *et al.*, "Measurement of the D^* polarization in the decay $B^0 \to D^*\tau^+\nu_\tau$," 2019. arXiv: 1903.03102 [hep-ex].

[26] B. Waheed *et al.*, "Measurement of the CKM matrix element $|V_{cb}|$ from $B^0 \to D^{*-}\ell^+\nu_\ell$ at belle," *Physical Review D*, vol. 100, no. 5, Sep. 2019. DOI: 10.1103/physrevd.100.052007.

[27] M. Blanke *et al.*, "Impact of polarization observables and $B_c \to \tau\nu$ on new physics explanations of the $b \to c\tau\nu$ anomaly," *Physical Review D*, vol. 99, no. 7, Apr. 2019. DOI: 10.1103/physrevd.99.075006.